# CYCLE-TO-CYCLE COMBUSTION VARIATIONS IN A SPARK-IGNITION ENGINE OPERATING AT IDLE

by

Peter Christopher Hinze

B.S.M.E., Massachusetts Institute of Technology

(1991)

M.S.M.E., Massachusetts Institute of Technology

(1993)

Submitted to the Department of Mechanical Engineering
in partial fulfillment of the requirements for the degree of
Doctor of Philosophy

at the

MASSACHUSETTS INSTITUTE OF TECHNOLOGY

September 1997



Author _____
Department of Mechanical Engineering
June 6, 1997

Certified by _____
Wai K. Cheng
Professor, Department of Mechanical Engineering
Thesis Supervisor

Accepted by _____
Ain A. Sonin
Department Graduate Chair

# CYCLE-TO-CYCLE COMBUSTION VARIATIONS IN A SPARK-IGNITION ENGINE OPERATING AT IDLE

by

Peter Christopher Hinze

Submitted to the Department of Mechanical Engineering
June 6, 1997 in Partial Fulfillment of the Requirements
for the Degree of Doctor of Philosophy

## ABSTRACT

Spark ignition engines at idle are particularly susceptible to cycle-to-cycle combustion variations, which result in objectionable engine noise and vibrations. The purpose of this work is to identify and quantify the major physical phenomena that contribute to cycle-to-cycle combustion variations at idle. Through consideration of the existing literature on cycle-to-cycle variations and the combustion environment of the idle operating condition, several important contributing factors were identified: in-cylinder turbulence, bulk fluid motion, and charge composition fluctuations. A quasi-dimensional modeling study suggested that both charge composition and turbulence intensity variations significantly influenced combustion variations, while bulk fluid motions exhibited a somewhat lesser effect.

A methodology was developed by which the measurable outputs of an engine (i.e., burn duration and IMEP) could be used to determine the variations in the charge (i.e., fuel mass, air mass, and residual mass) in a modern spark-ignition engine. A novel set of in-cylinder gas composition perturbation experiments were performed to determine the sensitivity of the combustion to small changes in the charge component gases: fuel, air and residual. Results of these experiments indicated that combustion was most sensitive to the fuel mass perturbation, followed by residual mass and air. These results were consistent with the quasi-dimensional modeling study.

A set of skip-firing experiments, in which the fuel, air, and residual mass variations were removed entirely showed that composition variations are a significant source of cycle-to-cycle variability at idle. The skip-firing experiments exhibited lower combustion variability than ordinary continuously-fired experiments; the earlier burn phases had the largest reduction in variability, whereas the later burn durations showed a smaller reduction in variability as a result of skip-firing. This is because, unlike charge composition variations, gas flow variations influence the later part of combustion much more than the earlier.

The results of the sensitivity experiments were used to determine the cycle-to-cycle variations in the charge component gas masses; the percent variations determined were as follows: air 5.5%, residual 4.4%, and fuel 0.6%. However, since the combustion is less sensitive to changes in air mass, residual mass was found to be the largest contributor to cycle-to-cycle combustion variations. The contribution of the air and fuel variations to the cycle-to-cycle combustion variability are of the same order.

**Thesis Advisor**
Wai K. Cheng
Associate Professor, Mechanical Engineering

## Acknowledgments

It is with great and sincere gratitude that I acknowledge my advisor Professor Wai Cheng for his assistance and guidance in making this thesis reality. His "no matter what the problem, it can be fixed" attitude helped through many a hard time. Sincere thanks to my committee members as well: Professors Zaichun Feng, John Heywood, Simone Hochgreb and James Keck. Their ideas and suggestions were invaluable.

My time at the Sloan Automotive Laboratory has been incalculably enriched by the many graduate students and visiting scholars that I have met and had the opportunity to work with. My gratitude goes to Professor Huixian Shen for his help with the cycle simulation code. Thanks also to Younggy Shin and Helen Liu for their flexibility in scheduling their time on the Nissan engine. Extra special jumbo thanks to Pete Menard and Brian Corkum for their expert help, advice, and general competence down in the lab; without you guys, this place would fall apart. Nancy Cook, that goes *double* for you. Finally, thanks to all of the friends who have made my time at the lab such a great experience; you will all be sorely missed.

My family has been a source of continuing support since I was a wee lad; thanks for your love and patience (and $). And Jen—my best friend, life-partner, and all-around amazing person—it is to you that I owe the greatest debt of gratitude. You are the best part of my life; without you, this would not have been possible. Last, but not least, I need to thank Atticus (C.G.F.T.P.U.) and Maisie (M.M.M.P.).

This work was supported by the Industrial Consortium for Engine Research. Member companies are Chrysler Motor Corporation, Ford Motor Company, General Motors Research, Peugeot S.A., Renault, and Volvo Car Corporation.

# Table of Contents

## Table of Figures

## Table of Tables

# 1. INTRODUCTION

**THESIS STATEMENT:** Idle operation in a spark-ignition engine constitutes a poor environment for a fast, repeatable combustion event. Since good idle quality is an important attribute of engine design, an understanding of the underlying phenomena that cause cycle-to-cycle combustion variations would be a useful design tool. The purpose of this thesis is to identify and quantify the phenomena that significantly contribute to cycle-to-cycle variations in combustion at idle. The focus will be upon the influence of overall charge composition variations on combustion variations.

## 1.1. Cycle-to-Cycle Combustion Variations

### *1.1.1. MOTIVATION*

Cycle-to-cycle combustion variability is a prominent characteristic of spark ignition engine operation. Changes in the combustion environment from one cycle to the next may result in significant variations in the combustion event. These cycle-to-cycle changes in combustion will be reflected in variations in the cylinder pressure, which will, in turn, be manifested as power variations. Depending on the severity of the combustion variability, these power variations may be objectionable to the driver, or they may only be detectable through precise measurement of the engine performance.

Cycle-to-cycle combustion variations represent a problem to engine designers for several reasons. Since satisfying the customer is the primary goal of any automobile manufacturer, the consumer's perception of engine "smoothness" is an important concern. Cyclic combustion variations result in non-uniform power delivery—uneven acceleration or a shaky idle condition, for example—that can be

felt by the driver; vehicle drivability suffers as a result. Also, studies have shown that cycle-to-cycle variations in the in-cylinder pressure contribute to engine noise [1]. While the driver's perception of engine smoothness and noise may be influenced by many factors apart from the actual combustion variations—e.g., sound and vibration damping, engine mounting, drivetrain vibration—reducing combustion variations is necessary from the standpoints of drivability and customer satisfaction.

Combustion variations are also responsible for penalties in engine performance. The spark timing for maximum brake torque (MBT timing) is optimized for an "average" cycle; any cycles that burn faster or slower than this average will not have the optimum burn schedule to produce peak power, thus causing a reduction in average power output. Also, to avoid knock the ignition calibration must leave a sufficient margin for cycle-to-cycle variations. Studies suggest that complete elimination of cycle-to-cycle combustion variations would result in up to a 10% improvement in power output for the same fuel consumption [2]. Additionally, cycle-to-cycle variations limit the range of conditions under which an engine may operate. This is of particular concern for lean or highly dilute operation, when combustion speeds are low and cyclic variability high. Since misfires and partial burn cycles[1] result in very high emissions and performance penalties, the lean/dilute operating limit is effectively set by the slowest burning cycles.

This thesis focuses on the engine cycle-to-cycle variations under the idle operating condition. At idle the environment is unfavorable to combustion because the charge is significantly diluted by residual gas. Also, torque fluctuations at idle are particularly objectionable to the driver because of the low frequency excitation of mechanical vibrations of the various panels in the passenger compartment. The objective of this thesis is to identify and quantify the sources of cycle-to-cycle

[1] A misfire is said to occur when the spark fails to create a self-sustaining flame kernel and little or none of the charge is burned. A partial burn cycle is a cycle in which the charge has not been consumed completely by the time the exhaust valve opens. This may be caused by flame quenching or simply by the exhaust valve opening before the combustion has completed due to a very slow burn.

combustion variations at idle. This information is crucial to engine design for the improvement of idle quality.

In the following section, the various factors that contribute to cycle-to-cycle combustion variations are briefly reviewed.

### *1.1.2. Previous Work*

There exists an extensive body of literature concerned with the problem of cycle-to-cycle combustion variations. Young [1] presented a thorough review of work before 1981; Ozdor, Dulger, and Sher [3] reviewed the more recent work done, and pointed out possible new avenues for research. Since both of these papers provide excellent reviews, and an extensive literature review is outside of the scope of this thesis, a more modest survey of the relevant work in the field will be presented.

Ozdor, et al., [3] presented a table that summarizes the causes of cycle-to-cycle combustion variations as found in the literature (Table 1-1). This table represents a concise overview of the results of many investigators, as well as areas that are unstudied. However, there are several complications in offering a summary of many different investigations in such a compact format. First of all, results of different investigators are often contradictory, so marking one factor as "significant" belies the fact that the results of different researchers are not always in agreement. Secondly, cycle-to-cycle combustion variations are, by necessity, dependent on the engine operating condition and geometry; what is significant at idle is not necessarily important at full load, and variations in an engine with a two valve hemispherical head may have a very different nature from those in a four valve pent-roof design. Additionally, the "causing factors," as they are listed on the table, give the impression of non-interacting phenomena; in truth, the turbulent fluid motion will influence the mixture homogeneity, the bulk flow velocity at the spark plug gap will affect the spark energy input, etc. Thus, the causing factor categories are not as separate as they may appear in the table. Nevertheless, Table 1-1 serves as a useful starting point to discuss the sources of cycle-to-cycle variations.

Table 1-1. Factors that cause cycle-to-cycle variations (c.c.v.) in combustion. [3]

| C.c.v. causing factor | Influenced combustion stage 1-sparking and flame initiation, 2-initial flame kernel development 3-turbulent flame propagation | Kind of caused primary variations | Relative contribution (asterisks stand for remarks listed beneath table) |
|---|---|---|---|
| turbulence intensity and scales | 2 | Flame stretching, local quenching, flame kernel convection | Significant |
| c.c.v. in the overall A/F ratio | 2 | Laminar flame speed, affecting flame kernel growth rate | * |
| | 3 | Laminar flame speed affecting flame propagation velocity | Unstudied |
| c.c.v. in the overall fraction of diluents | 2 | Laminar flame speed, affecting flame kernel growth rate | * |
| | 3 | Laminar flame speed affecting flame propagation velocity | ** |
| mixture spatial inhomogeneity | 2 | mixture composition in the "first eddy burnt" | Depends on scale of non-uniformities |
| c.c.v. in cylinder charging | 3 | Amount of fuel burned per cycle | Significant (conclusion based on a single study) |
| c.c.v. in mean flow vector | 1 | Length of spark channel affecting spark discharge characteristics | Small |
| | 2 | Kernel convection velocity vector | Small, *** |
| c.c.v. in spark discharge characteristics | 1 | Initial size of the hot plasma kernel | Unstudied, **** |
| | 2 | Energy amount and rate of its deposition into the flame kernel | Unstudied, **** |
| spark "jitter" | 1 | Thermodynamic conditions affecting spark breakdown energy | Negligible, particularly in modern electronic ignition systems |
| | 3 | Combustion phasing in the cycle | |
| Comments:<br>* Only a combined effect of spatial inhomogeneity and c.c.v. in both overall A/F ratio and fraction of diluents can be drawn from the studies with local mixture sampling; this combined effect is estimated to be significant.<br>** The effect is coupled with the effect of c.c.v. in cylinder charging (reduced amount of residuals in the cycle is usually accompanied by increased amount of fuel to be burned, thereby the effect is amplified). | | *** C.c.v. in flame kernel convection can be caused by both random turbulent fluctuations and c.c.v. in mean flow velocity. The latter source seems to be less important, therefore its contribution is estimated as small.<br>**** C.c.v. in spark discharge characteristics are mostly a secondary effect of the c.c.v. in mean flow velocity. There is a lack of data on the magnitude of these variations; only the effect of mean values of spark characteristics are reported. | |

### 1.1.2.1. Fluid flow effects

According to Table 1-1, the phenomena that cause cycle-to-cycle combustion variations may be divided up into three main categories: fluid flow effects, charge composition effects, and spark ignition effects. Fluid flow effects include turbulence intensity and scales and the mean flow vector. Cycle-to-cycle variations in the mean flow vector will cause cyclic variations in the interaction of the flame kernel with the combustion chamber geometry—i.e., the combustion chamber walls and the spark plug. The variations will influence combustion by affecting the heat transfer from the flame and the burned gases to the combustion chamber, and the flame area, which affects the burning rate proportionally. In the case of very high flow velocities in the vicinity of the spark gap, the flow stretches the discharge channel, increasing the impedance across the gap; this results in a smaller energy input into the kernel from the spark during the low current discharge. Depending on the characteristics of the ignition driver, a new breakdown arc may occur [4]. Since bulk flow velocity influences the ignition process and flame growth in so many ways, it follows that cycle-to-cycle variations in the bulk flow will result in variations in combustion. Many studies have reported that there is a significant relationship between mean flow in the vicinity of the spark gap and combustion variability in the early flame kernel development [4, 5, 6, 7, 8, 9]. Since the development of the kernel necessarily affects the overall combustion schedule, in-cylinder mean flow variations should also influence the overall cycle performance—e.g., indicated mean effective pressure (IMEP)[2]. Through in-cylinder imaging, Bates found that in certain cases the overall shape of the flame kernel may persist intact throughout much of the main combustion phase[3], causing a large penalty in burn rate in the case of certain "cleft-flame" cycles [4]; these results were

---

[2] IMEP is a measure of the work output of an engine; it is the work output per cycle divided by the displaced volume, giving a dimension of pressure.

[3] Used in this sense, the main combustion phase is considered to begin after the kernel has fully developed into a turbulent flame and end when the entire combustion chamber volume has been enflamed. It roughly corresponds to the rapid burning angle (10-90% mass fraction burned angle) defined by Heywood [23], though I intentionally use it in a less precise manner to represent the period of combustion that is dominated by turbulent flame propagation.

only noted at 500 RPM, however, which is slower than an ordinary engine would operate.

Cycle-to-cycle variations in the turbulence intensity and scales, as well as the inhomogeneity of the turbulence in the cylinder, will influence the development of the flame. Turbulence primarily affects the flame in a spark ignition engine in two ways: it wrinkles the flame, creating more surface area and thus increasing the flame speed; and it strains the flame locally, possibly causing flame slowing and quenching, particularly in the case of lean and dilute operation [10, 11]. However, the flame kernel does not start as a fully-developed turbulent flame. Before the flame kernel reaches the size of the integral length scale, turbulence will convect the kernel on a sort of "random walk" [9, 12], the path of which is determined by the random interaction of the small flame kernel with turbulent eddies in the vicinity of the spark gap. Experiments indicate the flame kernel is initially laminar [9, 13, 14, 15], though it does not take long for the flame surface to be influenced by turbulence; studies have shown that turbulence may affect the kernel before 0.5 percent of the charge mass has been consumed [7, 16, 17, 18]. How early the flame is affected by turbulence is influenced by the turbulence scales in the vicinity of the spark plug: the smaller the turbulent eddies, the more quickly the laminar flame kernel will make the transition to a turbulent flame [19, 20]. Turbulence scale variations will affect the early flame development by causing variations in the time it takes for the kernel burn rate to become enhanced by turbulent wrinkling of the flame surface, and turbulence intensity variations will cause variations in the subsequent development of the wrinkled flame.

The influence of turbulence on the flame speed is especially significant from the time the kernel has developed into a turbulent flame until the entire cylinder contents have been entrained by the turbulent flame brush [21, 22, 23, et al.[4]]—a

[4] Heywood offers a good summary of turbulent flame modeling in engines in "Combustion and its Modeling in Spark-Ignition Engines," The Third International Symposium on Diagnostics and Modeling of Combustion in Internal Combustion Engines, July 11-14, Yokohama, Japan, COMODIA 94, pp. 1-15, 1994.

period of time that represents up to 80% of the entire combustion duration. In what is probably an oversight, Ozdor, et al. [3] do not list variations in turbulence intensity and scales as a possible source of combustion variability in the turbulent flame propagation stage in their table. It is true that since turbulence intensity measurements are typically local, most studies of the influence of turbulence variations on combustion are limited to kernel development, where the spatial volume of interest is very small; thus, data for the main combustion period are limited. However, some work has been done to attempt to relate bulk turbulence and combustion speeds during the later phases of combustion. Through simultaneous laser Doppler velocimeter (LDV) and ionization probe measurements in an engine, Witze, Martin, and Borgnakke [24] found that there was a strong correlation between the cycle-to-cycle variations in turbulence intensity ahead of the flame and flame arrival time at the LDV probe volume, suggesting that fluctuations in the bulk turbulence intensity ahead of the flame cause variations in burn rate during the main combustion phase. Keck and coworkers [9], on the other hand, found no evidence of variations in turbulence intensity and scales during the main combustion stage; however, these quantities were not measured directly in the experiments—rather, they were calculated through the application of a semi-empirical combustion speed model matched to simultaneous high-speed Schlieren movies and in-cylinder pressure measurements. Thus direct comparison with the results of Witze, et al. is difficult.

#### 1.1.2.2. Mixture composition effects

The laminar burning speed of a mixture of fuel, air, and residual uniquely depends on the relative concentrations of these components (as well as mixture temperature and pressure); many investigators have experimentally determined the relationship between charge composition and laminar burning speed for various fuel/air/diluent mixtures [25, 26, 27, 28, et al.], with Bradley, et al. offering a good summary and generalization for liquid fuels [29]. Even though, for the majority of the combustion event, the flame in an engine is not laminar, the laminar burning

speed is an important determinant of the overall burn rate. Thus, any cyclic variations in mixture composition, whether global or local, should contribute to cycle-to-cycle variations in combustion.

Unfortunately, in-cylinder mixture composition measurements suffer from a similar problem to in-cylinder velocity measurements: they are typically local in their sample volume, so attempting to apply these measurements to any stage of combustion other than early flame development remains a challenging task. Application of laser induced fluorescence (LIF)[5] does enable the acquisition of a two-dimensional cross-sectional image of the distribution of fuel—or, more precisely, fuel dopant—in the combustion chamber; there have been a significant number of studies in which LIF was successfully applied to an engine to visualize large scale fuel distributions [30, 31, 32, 33]. Berkmüller et al., [33] have used LIF to visualize residual gas concentrations by measuring nitric oxide (NO) concentrations in the fresh charge. There are various difficulties in applying this technique to cycle-to-cycle variations; most important, perhaps, is the low signal to noise ratio, which makes acquisition of single cycle images a challenge [32]. In studies where LIF was successfully employed to investigate cyclic combustion variations, the correlations found between combustion and fuel concentration are invariably only significant over a small area of interest because, as the flame gets larger, a two-dimensional LIF image is insufficient to characterize the mixture strength for the entire flame [8, 33].

There have been many investigations on the influence of mixture composition in the vicinity of the spark gap on combustion variability. Hamai et al., by using a spark plug with an integrated sampling valve, found that there were significant variations in air-fuel ratio near the spark gap and that these variations correlated with initial flame development as well as IMEP [34]. LeCoz et al., found a significant correlation between the cycle-to-cycle variations in local fuel and

[5] Also written as PLIF (planar laser induced fluorescence).

residual concentrations measured by LIF and the 0-5% mass fraction burned duration [8, reported in 35]; depending on spark timing, these mixture concentration variations could account for 15% to over 50% of the variations in the 0-5% burn duration. Through 2D LIF measurements in a plane near the spark plug, Berkmüller et al., [33] found that fuel concentration in the vicinity of the spark plug does influence combustion variations in the early flame development. On the other hand, Lee and Foster [36] found through simultaneous Rayleigh scattering, fiber-optic spark plug, and cylinder pressure measurements, that fuel concentration variations at the spark gap did not contribute to combustion variations.

Local sampling techniques do not allow for the separation of mixture homogeneity effects and overall variations in the charge composition. A few investigators have attempted to characterize the influence of overall charge inhomogeneity on cycle-to-cycle combustion variations. In a very thorough study, Sztenderowicz [37] attempted to characterize the influence of charge composition nonuniformities on combustion variations; in his work, he considered the effects of fuel/air nonuniformities and residual/fresh charge nonuniformities. His results indicated that there was no reduction in combustion variability with a homogeneous charge, though he comments that this result may not be valid for operating conditions other than those used in his study—MBT spark timing and stoichiometric operation. Sztenderowicz's result is consistent with that of Berckmüller et al., [33] who found no correlation between fuel concentration nonuniformities and combustion variability in the later periods of the combustion event (i.e., after the kernel has grown to a size that is large in comparison to the scale of inhomogeneities); Berckmüller et al., attributed this result to the mixing out of inhomogeneities as the cycle progresses and the averaging of local fluctuations in fuel concentration over a large flame front.

The variation in the overall charge composition is a subject that has not received enough attention according to the review of Ozdor, Dulger and Sher. The overall amount of fuel/air/residual should be an important contributor to cycle-to-

cycle variations for similar reasons that the local concentrations are important. Additionally, cycle-to-cycle variations in the total fuel mass will influence the total energy release, and thus should effect the IMEP variability [37]. Grünefeld et al., [38] used spontaneous Raman scattering to measure the spatially integrated densities of fuel, oxygen, nitrogen and water in a 1.4 $cm^3$ probe volume on a cycle-to-cycle basis. They found that there were significant variations in the overall residual mass concentration and equivalence ratio, and that these variations could be linked to combustion variations. They also noted very strong prior-cycle effects: a slow combustion cycle would follow a fast combustion cycle, and vice-versa. The reason for this effect, they noted, was the density change in the residual gas. That is, a fast burning cycle would result in a low residual gas temperature and, thus, high residual gas density. The next cycle, because of the high residual density of the previous cycle, would have a high residual content, leading to a slower burning cycle with a high residual gas temperature. The next cycle is a fast burn, because of the high residual temperature and low density. Thus, a strong/weak cycle pattern is established. Many investigators have noted such a pattern [39, 40, 41], and Stevens, Shayler, and Ma have attempted to use predictive control of cycle-to-cycle variations by using prior-cycle patterns [42].

#### 1.1.2.3. Spark Ignition Variations

Table 1-1 shows two categories whereby the process of spark ignition may introduce combustion variations. "Spark jitter," that is, small variations in spark timing introduced by the ignition system, is thought to be insignificant with modern electronic ignition systems; the influence of jitter may have been larger in conventional point-breaker ignition systems. Variations in spark discharge characteristics, as noted in the table, are mostly a secondary effect of bulk flow in the spark plug gap lengthening the spark channel; in their review, Ozdor et al., note that this effect is small. The existing work on spark ignition quality and variations in the spark process indicates that, provided the spark is strong enough to create a self-sustaining kernel, the ignition process does not significantly contribute to cyclic

variations in combustion [13, 43]; thus, as long as the engine is not operating at the misfire limit, the spark ignition process does not seem to introduce cyclic variability.

## 1.2. The Idle Operating Condition

At idle a spark-ignition engine is producing very little mechanical work: just enough to keep the engine and accessories running. In fact, much of the fuel energy at idle goes out the tailpipe as exhaust enthalpy. An ideal strategy at idle would meet the following criteria:

- adequate power for the accessories
- low fuel consumption
- high exhaust enthalpy flux (to keep the catalyst at temperature)
- smooth engine operation.

The engine system constrains the fulfillment of these goals. In particular

- the engine must operate at stoichiometric for the catalyst
- valve timing for maximum power at high speed requires high valve overlap.[6]

Typical modern engines operate with substantially retarded spark timing with respect to MBT. There are several reasons for this

- high exhaust gas temperature
- lower residual gas fraction (due to above)
- lower torque to control the engine speed (especially important in the case of low friction engine designs).

To achieve the goal of low fuel consumption, one may consider reducing the mass throughput of the engine; this could be achieved by reducing inlet pressure and/or engine speed. However, reducing either of these will result in higher residual gas dilution and poor combustion quality. Furthermore, consistent fuel metering at small quantities may be problematic for current fuel injector

[6] Valve overlap is the period where both the intake and the exhaust valves are open. At high speeds and loads a certain amount of valve overlap is desired for maximum power.

technology. Thus, setting the idle condition requires a compromise between achieving the listed goals.

The operating environment at idle is very unfavorable for a fast, robust combustion event. Of particular importance is the high dilution by residual which occurs because of the low inlet pressure and low engine speed at idle. In the past, engines tended to idle slightly rich of stoichiometric to reduce combustion variations; the fuel consumption and catalyst constraints preclude the use of that strategy today. In fact, due to the many constraints on the engine, the idle condition for modern engines is at or close to the dilute limit [44]. It is at this limit that cycle-to-cycle combustion variations may be their most severe [3].

## 1.3. Focus and Structure of This Thesis

### *1.3.1. THESIS FOCUS*

As indicated in the thesis statement, the purpose of this work is to identify and quantify the most important phenomena that contribute to cycle-to-cycle combustion variations at idle. However, considering the body of previous work presented in §1.1.2, it is clear that all possible contributing phenomena cannot be investigated in detail. Therefore an attempt was made, through careful consideration of the literature and the specific operating condition of idle, to distinguish the factors that contribute to cyclic combustion variability that would probably be the most significant at idle. These factors are as follows:

- variations in charge fluid motion
  - turbulence
  - bulk flow
- variations in the overall charge composition
  - residual
  - fuel
  - air.

Variations in charge turbulence may be particularly important at idle because high dilution makes the flame much more susceptible to quenching by turbulence [10, 11]. Also, turbulence is thought to have a direct influence on the combustion rate during a period over which more than 90% of the fuel mass is consumed; it is impossible to investigate the primary causes of combustion variability without considering the influence of turbulence. Bulk fluid motion effects, which influence the interaction of the flame with the spark plug and combustion chamber geometry,

are generally thought to be more important when operating near the dilute limit [3].

Cycle-to-cycle variations in residual mass will most likely be an important factor at idle for several reasons. Laminar burning speed is a very sensitive function of residual mass in the range of residual dilution that is present at idle (on the order of 30% of the charge by mass). There are three mechanisms that are thought to contribute to cycle-to-cycle variations in residual mass: exhaust valve leakage, variations in valve overlap due to hydraulic lash adjuster dynamics, and exhaust gas temperature fluctuations. Valve leakage occurs as a result of small amounts of deposits on the exhaust valve; this causes the valve to seat improperly, thus allowing exhaust gases to leak in from the exhaust port during the intake stroke. Hydraulic lash adjusters, which use the engine lubricating oil pressure to keep a certain amount of "slack" in the cam/valve/lifter assembly, are susceptible to pulses in the oil pressure, which will result in variations in valve timing from cycle to cycle. Since valve overlap is a determining factor in how much residual there is in the charge, any variations in valve timing will cause variations in residual mass. The influence of valve leakage and hydraulic lash adjusters on cycle-to-cycle variations will be more significant at idle than they would be under a higher speed and load condition because the low speed and low inlet manifold pressure at idle would tend to magnify those effects.

The order of magnitude of the transport of burned gas from the exhaust manifold back into the cylinder due to valve leakage may be estimated by assuming choked flow for a given valve seat leakage clearance. Typical values are shown in Table 1-2. The leakage effect could significantly change the residual gas mass in the charge. For reference, at idle (800 RPM, 0.32 bar inlet

Table 1-2. Burned gas leakage from exhaust to cylinder as a function of valve leakage gap δ.

| δ | $\Delta m_{leak}$ | $\Delta m/m_{charge}$ | $\Delta m/m_{residual}$ |
|---|---|---|---|
| 1 μm | 0.5 mg | 0.4% | 1.5% |
| 10 μm | 5 mg | 4% | 15% |

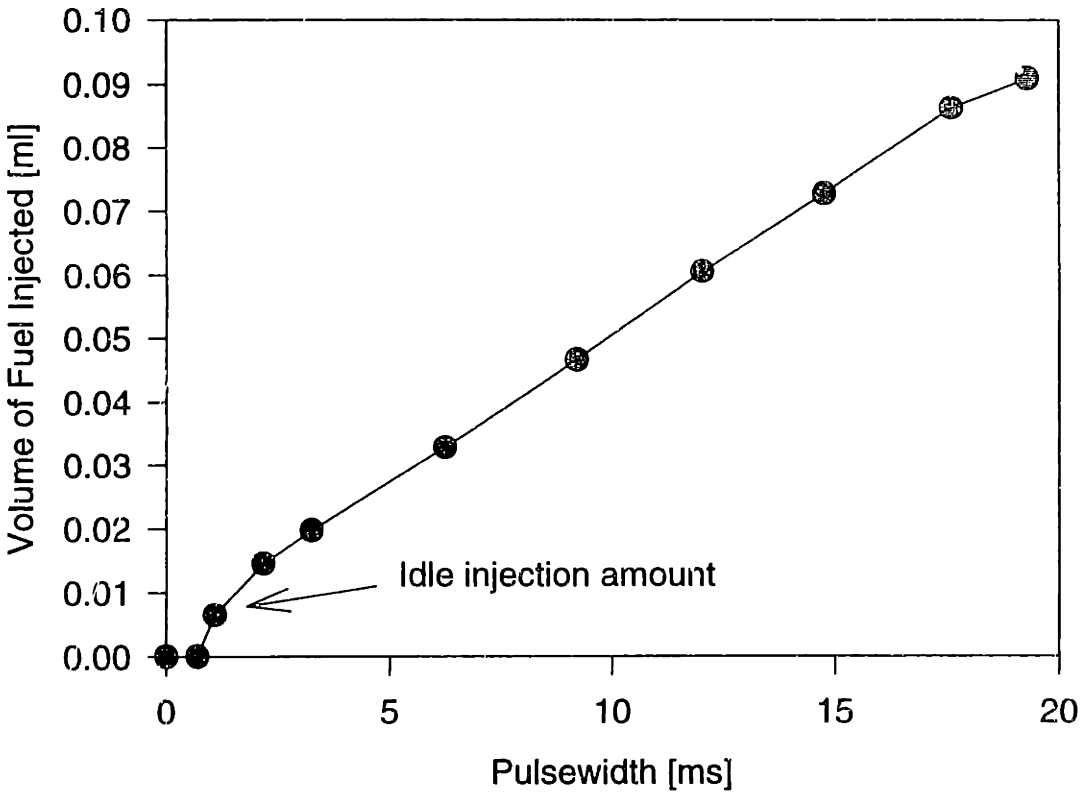


Figure 1-1. Fuel injector characteristic for Nissan SR20DE.

pressure), the cylinder contains ~90 mg air, 6 mg fuel, and 34 mg residual gas.

Variations in the overall fuel mass were judged to be of interest because of the very small fuel injection masses at idle. Fuel injection amounts may be lower than 0.01 ml per cycle at idle; shot-to-shot variability is inevitable at such low injection amounts. Figure 1-1 shows the injector characteristic curve for the Nissan SR20DE, the engine used in the experiments in this study. At idle for this engine, the fuel injection amount is about 0.0085 ml. The figure shows that this is at the non-linear part of the injector curve, where fuel injection amount is very sensitive to pulsewidth and mechanical jitter of the injector solenoid action; thus, operating in this region increases the tendency towards higher cycle-to-cycle variability in fuel mass. Fuel mass variations will influence the flame speed, as well as the total amount of fuel energy available.

Finally, variations in air mass were included in this investigation for two major reasons. First, due to the low inlet manifold pressure at idle, there is a very high amount of blowback of residual gases when the intake valve opens. The cylinder charging process is complex because the residual gases will displace or mix with the fresh charge, thus influencing the amount of air entering the cylinder. Also, valve leakage may allow some of the fresh charge to escape the combustion chamber during the compression process. Thus, there are plausible sources of variability in the total mass of air. Grünefeld et al., found evidence that there were variations of air mass in the charge on a cycle-to-cycle basis [38].

### *1.3.2. THESIS STRUCTURE*

This thesis is divided into seven chapters. Chapter 2 describes the adaptation and application of a quasi-dimensional engine cycle model to the problem of cycle-to-cycle variations. From the modeling study, sensitivities of the combustion to perturbations in the important parameters at idle—as described in §1.3.1—were identified. Chapter 3 presents the methodology of a novel set of gas perturbation engine experiments and skip-firing baseline experiments to assess the sensitivity of the combustion event to the charge components. Chapter 4 describes the test apparatus for the experimental portion of this work and characterizes the engine at the idle condition. Chapter 5 describes the experimental procedures, and Chapter 6 presents the results and error analysis from the engine experiments. Finally, Chapter 7 summarizes the significant findings and conclusions of this thesis.

# 2. Application of a Quasi-Dimensional Cycle Simulation to Cycle-to-Cycle Variations

## 2.1. Background

Chapter 1 summarized the literature on the phenomena that are believed to contribute to cycle-to-cycle combustion variability. One method of determining whether a particular factor (e.g., fuel concentration) is important is to measure the variations in that variable and correlate those results with combustion variations; this has been performed successfully in a number of studies [7, 8, 24, 34]. The difficulty in these experiments lies in the fact that the "cause" variable of interest comes from the natural processes of the engine and may not be independently controlled. For example, the fuel in the cylinder for a cycle is not the fuel injected, but is determined by a complex mixture preparation process. Thus, it is necessary to directly measure the "cause" variables in the cylinder for the cycle. The problem with this methodology is that the measurements are usually local and pointwise, so that the *overall* impact of a particular variable cannot be deduced. Thus, attribution of variations in delivered power is impossible, since the power depends on an integration of the cylinder pressure over the entire cycle, and cycle-to-cycle correlations between short periods of the combustion and the IMEP are invariably not significant. Another methodology for investigating the importance of a certain

factor on cycle-to-cycle combustion variability is to attempt to control—or completely eliminate—the fluctuations in one particular variable [37]. The weakness of this technique is that it may only be used for certain phenomena; it is impossible to eliminate variability in the turbulence intensity, and thus it is impossible to investigate the influence of turbulence intensity using this methodology.

These difficulties, as well as the large amount of experimental effort that must go into measuring most in-cylinder phenomena, have led many investigators to attempt to apply engine simulation models to the problem of cycle-to-cycle combustion variability [45, 46, 47, 48, 49, 50]. The methodology for such an investigation is straightforward. A deterministic engine cycle simulation that can accurately calculate the mean combustion parameters for various operating conditions serves as the basis. To perform a calculation, these simulations require certain "inputs" that will be used to determine the combustion rate and the pressure history of the cycle. These inputs generally include the variables that the engine operator would set if s/he were performing an actual engine test: inlet pressure, equivalence ratio, spark timing, etc. Also, depending on the simulation, the user may have control over additional variables—turbulence intensity and scales, bulk flow velocity and direction, etc. Perturbations in these "input variables" will result in changes in the model "output" variables such as combustion speeds and IMEP. As outlined in Chapter 1, these controllable input variables are among the phenomena that are thought to be important contributors to cycle-to-cycle combustion variations, so variations in these inputs to the model may be used to simulate the natural variations in the relevant phenomena in an operating engine. Since the operator has control over the variations in these inputs, it is possible to determine individually the influence of each on the variability in the engine outputs. Figure 2-1 shows a schematic for this methodology. The input parameters listed are not necessarily the only possible contributors to cycle-to-cycle variations.

There have been several ways in which this methodology has been implemented. Brehob and Newman [46] perturbed three model inputs—initial kernel burn rate, displacement of the kernel from the spark gap, and turbulence intensity—until they achieved output distributions that approximated actual engine experimental results for burn rate and IMEP. Shen et al., [49] used data from a fiber optic spark plug as input for the cycle-to-cycle variability in the in-cylinder flow characteristics. Holmström and Denbratt [48] used LDA measurements of mean velocity, turbulence intensity and integral length scale as inputs to an engine simulation to model the influence of the kernel's "random walk" on combustion variations. Other investigators use distributions in the inputs simply as an "excitation" to determine the influence on cycle-to-cycle variations.

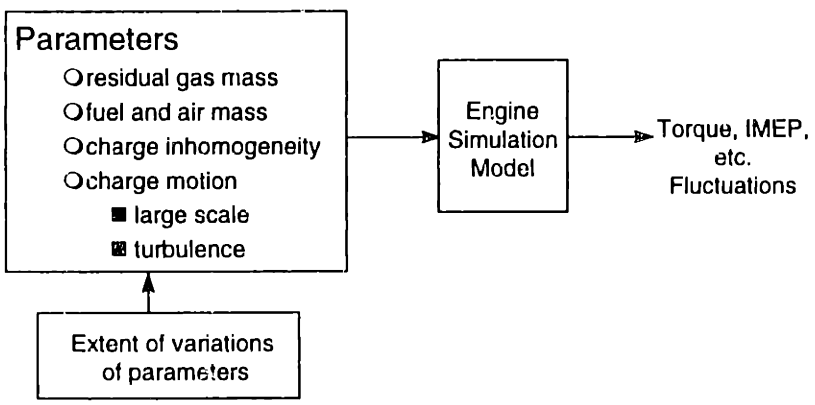


Figure 2-1. Methodology for modeling cycle-to-cycle combustion variations.

## 2.2. The Quasi-Dimensional Cycle Simulation

### *2.2.1. The Basic Model*

The basic model used for the calculations in this study is a quasi-dimensional cycle simulation developed by Poulos [51, 52]. Additional features were introduced for the purpose of this study; these features will be described subsequently. The basic model has been described in detail in the aforementioned publications, so only a summary of its features will be presented here.

The simulation uses a two-zone thermodynamic model of the combustion. The unburned zone is assumed to be a homogeneous mixture of fuel, air, and residual gas at a uniform temperature throughout the cycle; the composition is assumed to be frozen. During combustion, the burned zone is modeled as a homogeneous mixture of ideal gases in chemical equilibrium at a mean temperature. For $NO_x$ calculations, the burned zone is divided into an adiabatic core and a boundary layer, though this feature does not significantly influence the thermodynamics of the calculation. Pressure is considered to be spatially uniform throughout the cylinder at all times. The combustion model used is an eddy entrainment and burn-up model that has been described extensively in other publications [21]. The simulation accounts for the influence of the chamber geometry on the combustion by assuming that the flame is a sphere, the center of which is fixed at the location of the spark discharge; as this sphere contacts the walls, the flame area is reduced and the heat transfer area between the burned gases and the combustion chamber walls is increased.

The original cycle simulation converges on a solution by calculating several cycles in sequence, using the end conditions of one cycle as the starting conditions of the next. In this way it is analogous to a continuously-fired engine: the residual gases from one cycle are left over for the next. Thus, when the simulation is used to calculate many cycles in sequence, the residual mass, total charge mass, and in-

cylinder pressure and temperature vary naturally. However, since the cylinder charging subroutine does not allow for mixing or heat transfer between the unburned charge and the residual gas during the backflow and intake processes, the accuracy with which the program calculates cylinder charging is suspect.

### *2.2.2. MODIFICATIONS*

Shen, Hinze and Heywood [49] presented a modified cycle simulation and applied it to the modeling of cycle-to-cycle variations. The simulation code used in this thesis is, except in one respect, identical to the model presented by Shen et al. Thus, the details of the simulation will only be summarized here.

#### 2.2.2.1. Flame Kernel Model

The original quasi-dimensional cycle simulation initiates the combustion by specifying the size and temperature of the original flame kernel; this initial condition does not change from cycle-to-cycle. However, cycle-to-cycle variations are believed to begin very early in the cycle. To allow for the variations in very early flame development, a flame kernel model was added to the simulation to provide the initial condition for the main combustion phase calculated by the simulation. The kernel model is applied for the entire spark duration, at which point the simulation takes over.

The kernel model added to the simulation is that of Shen, Hinze and Heywood [53]. The model takes into account the primary physical factors that influence early flame development. The initial kernel size and temperature are determined by the breakdown energy and the heat transfer from the burned region to the unburned region, and the calculation for flame development considers the heat losses to the plug electrodes, energy input from the spark, and the development of the kernel from initially laminar to a wrinkled flame. The model allows the kernel to be convected from the center of the spark gap. This will influence the heat transfer between the kernel and the spark electrodes and the interaction of the flame with

the combustion chamber walls during the later phases of combustion. The direction of convection is limited to the plane perpendicular to the cylinder axis.

### 2.2.2.2. Turbulent Flame Speed Model

The turbulent entrainment combustion model used in the study by Shen et al., [49] was replaced with an expression adapted from Herweg and Maly [54]. In this model, they use a turbulent flame speed expression

$$\frac{S_t}{S_l} = I_0 + I_0^2\left(\frac{u'}{u'+S_l}\right)^{1/2}\left(1-\exp\left(-\frac{r_k}{L}\right)\right)^{1/2}\left(1-\exp\left(-\frac{t}{\tau_{0G}}\right)\right)^{1/2}\left(\frac{u'}{S_l}\right)^{5/6} \qquad (2\text{-}1).$$

In this expression $S_t$ and $S_l$ are the turbulent and laminar flame speeds respectively, $I_0$ represents the flame strain, u' is the turbulence intensity, $r_k$ is the radius of the flame, L is the integral length scale, t is the time after spark, and $\tau_{0G}$ is a characteristic time scale. The flame strain is given by the following equation:

$$I_0 = 1-\left[\left(\frac{\delta_l}{15L}\right)^{1/2}\left(\frac{u'}{S_l}\right)^{3/2} + 2\frac{\delta_l}{S_l}\frac{1}{r_k}\frac{dr_k}{dt}\right]\left\{\frac{1}{Le}+\left(\frac{Le-1}{Le}\right)\frac{T_a}{2T_{ad}}\right\}$$

where $\delta_l$ is the laminar flame thickness, Le is the Lewis number, $T_a$ is the activation temperature, and $T_{ad}$ is the adiabatic flame temperature. The characteristic time scale is given by the following equation:

$$\tau_{0G} = \frac{L}{u'+S_l}.$$

This model was developed to account for the influence of turbulence on the flame kernel development explicitly; the turbulent flame speed multiplied by the flame area and the unburned gas density will yield the turbulent combustion rate. When the flame reaches the combustion chamber walls, however, the flame frontal area concept is no longer applicable; the remaining portion of the combustion may be modeled as burn-up of small pockets of unburned gas behind the flame front.

To incorporate the entrainment and burn-up concept into the Herweg and Maly flame speed model, the following equations were used in the simulation [55]:

$$\dot{m}_b = \rho_u A_f S_l I_0 + \frac{m_e - m_b}{\tau_b} \qquad (2\text{-}2)$$

$$\dot{m}_e = \rho_u A_f \left[ S_l I_0 + I_0^{1/2} u' \left(\frac{r_k}{L}\right)^{\frac{1}{3}} \left(\frac{\rho_u}{\rho_b}\right)^{\frac{1}{2}} \left(1 - \exp\left(-\frac{r_k}{L}\right)\right)^{1/2} \left(1 - \exp\left(-\frac{t}{\tau_{0G}}\right)\right)^{1/2} \right] \qquad (2\text{-}3)$$

I II III IV

Here, $m_b$ is the burned gas mass, $m_e$ is the mass of gas entrained behind the flame front, $\rho_u$ and $\rho_b$ are the unburned and burned gas densities respectively, and $A_f$ is the flame front area. Equation (2-2) is the standard form of the eddy entrainment and burn-up combustion model [21] with an added factor to account for the influence of strain on the burn rate. In this equation, $\tau_b$ is a characteristic eddy burn-up time:

$$\tau_b \propto \frac{L}{S_l}$$

Equation (2-3) is made up of four distinct terms, labeled I-IV above: a strain term, a turbulence factor, a size dependent integral length scale, and a time dependent integral time scale. Expressions III and IV are meant to represent the development of the combustion from a laminar kernel to a fully developed flame; when the kernel is small, the scales of turbulence are too large to significantly wrinkle the flame surface, but as the flame grows larger, the speed at which it propagates becomes more and more influenced by turbulence.

Herweg and Maly verified the application of this flame speed model for a variety of operating conditions in a specially designed transparent side chamber engine. Dai et al. [55], demonstrated that use of this model resulted in improved prediction of combustion rates for lean and dilute mixtures in Ford's quasi-

dimensional engine simulation (GESIM). Moreover, Dai et al., observed that the influence of flame strain was important at lean and dilute operation.

### 2.2.2.3. Flame Interactions With the Combustion Chamber

To simulate the random interactions of the flame with the combustion chamber geometry, the flame center is allowed to move from the center electrodes. The kernel model described in §2.2.2.1 also requires a convection velocity as an input; this velocity affects the contact area of the kernel with the spark plug electrodes. Early in the combustion, when the kernel is small, the bulk flow velocity of the charge may have a significant effect on the kernel motion. However, as the flame grows larger, the kernel is less influenced by the in-cylinder flows; thus, as the flame gets larger, it asymptotically approaches a stable center. Shen et al., [49] use an expression developed from results from experiments in a transparent cylinder engine [56] to model the relationship between the flame center offset and the flame radius:

$$r_{cs} = \sigma_c \left( 1 - e^{-\frac{r_f}{5.7}} \right)$$

$$\sigma_c = 5.7 \frac{v_c}{S_g}$$

Here, $r_{cs}$ is the distance of the flame center from the spark plug electrodes, $r_f$ is the flame radius, $v_c$ is the flame kernel convection velocity, and $\sigma_c$ is the final center of the flame when it stabilizes. Visualization engine experiments have verified the applicability of such an expression for flame center position as the combustion develops [9, 56].

The flame interactions with the combustion chamber primarily influence the combustion in two ways: heat transfer from the burned gases to the chamber walls, and flame front area, which directly influences the burn rate. Shen et al., developed a method whereby the flame front area during the cycle could be determined with little computational time for variations in the flame center position [49]. This

method involves dividing up the spherical flame area into 100 facets distributed on the flame surface. For each time step in the flame development process, the center point of each facet is checked to determine whether it is within the bounds of the combustion chamber. If the center point of a facet is still in the combustion chamber, the area of that facet is added to the overall flame area used to calculate burn rate. For a more detailed explanation, refer to Shen et al., [49].

### *2.2.3. MODEL CALIBRATION*

Before the model may be used to simulate the idle condition, it must be calibrated. To get the correct amount of mass in the cylinder and match the compression pressure of idle data, the inlet pressure must be adjusted. Also, it was necessary to add external EGR in the simulation because the model underpredicted the amount of residual in the cylinder. Finally, Equation (2-3) requires a turbulence intensity, u', and an integral length scale, L. These two parameters were chosen to match the pressure and burn rate data from actual experiments; a value of 1.0 m/s was chosen for u'[7], and L was chosen to be 3.5 mm. Figure 2-2 and Figure 2-3 show a comparison of the model results and sample idle cycles. A comparison with individual cycles from experiment is preferred to average cycle results because at a condition such as idle, the ensemble averaged cycle pressure does not necessarily represent typical engine performance [40].

[7] The mean piston speed is 2.3 at 800RPM, so this value for u' is approximately half the mean piston speed.

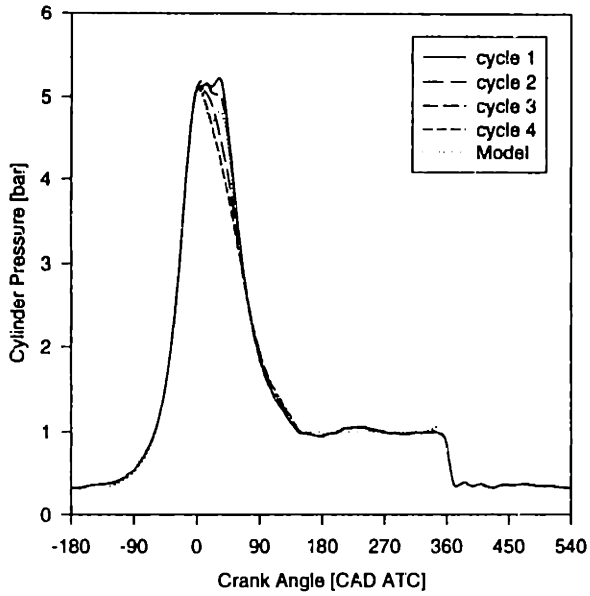


Figure 2-2. Comparison of model pressure trace and 4 sample idle cycles.

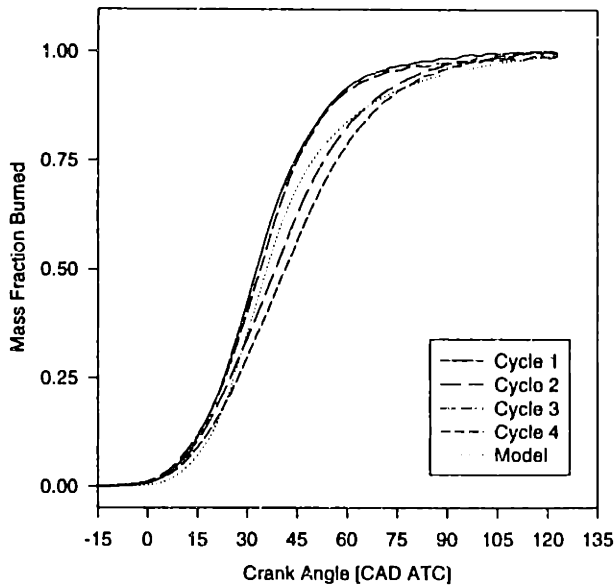


Figure 2-3. Comparison of model burn profile and 4 sample idle cycles.

## 2.3. Model Results

### 2.3.1. *Variability Tests*

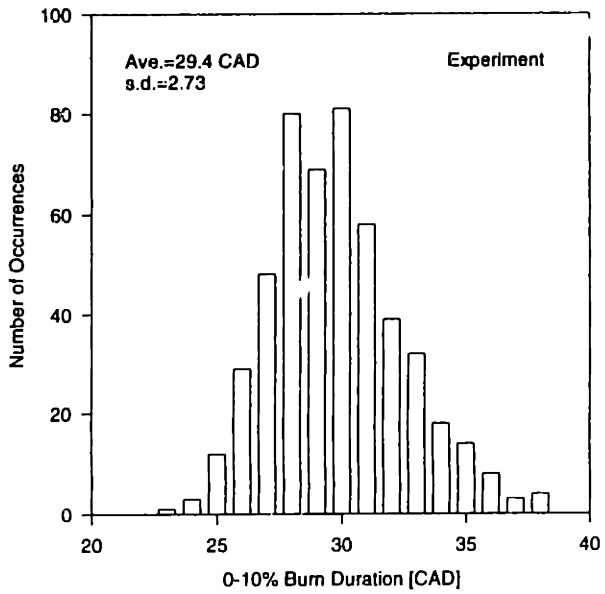


Figure 2-4. Distribution of 0-10% burn duration for 500 cycles at idle.

Figures 2-4 through 2-6 show typical results for the distribution in the 0-10%, 10-50%, and 50-90% burn durations (in crank angle degrees) at idle; 500 cycles are shown. To simulate the effect of variations in the influencing factors, a test distribution was used in the cycle simulation for turbulence intensity, convection velocity, and residual mass, and the effect on the different burn angles was observed. In each case, the input parameter was varied individually. It is important to note that

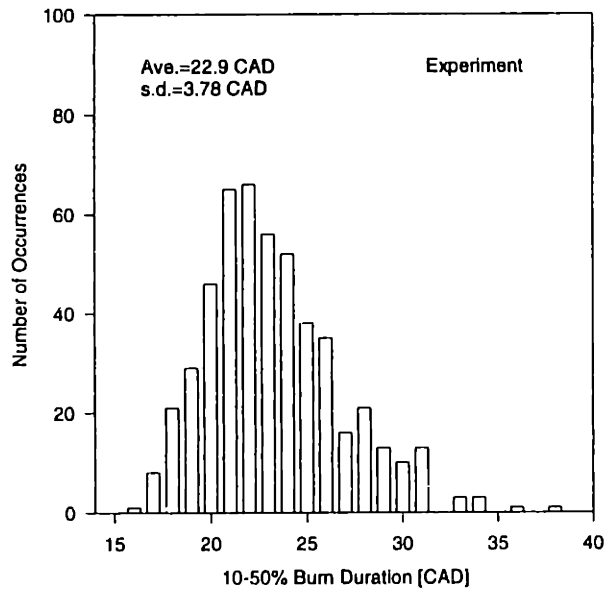


Figure 2-5. Distribution of 10-50% burn angle for 500 cycles at idle.

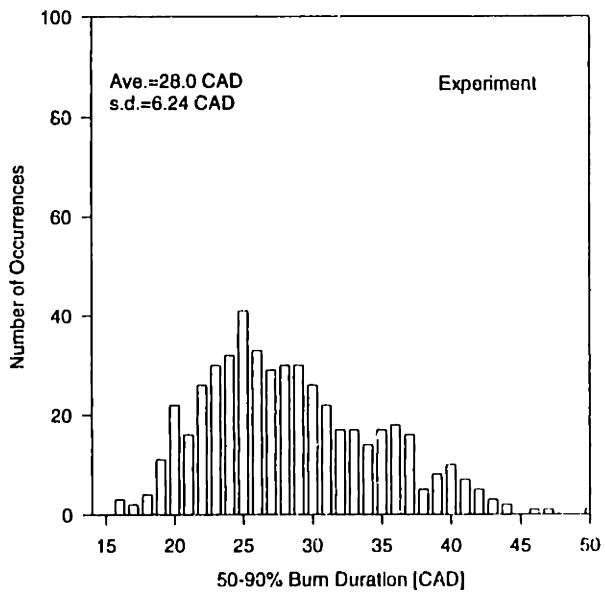


Figure 2-6. Distribution of 50-90% burn angle for 500 cycles at idle.

the input distributions used were chosen arbitrarily and do not necessarily represent the actual variations in the physical parameters in an engine.

Figure 2-7 shows the input distribution for the turbulence intensity, and Figures 2-8 through 2-10 show the resulting burn variations. Qualitatively, the modeled distributions appear to have similar features to the observed variations in engine tests. The average 10-50% burn angle for the simulation is shorter than the experimental value, presumably due to inadequacies in modeling the turbulent burn speed at that portion of the burn curve. The variations in the modeled 10-50% burn angle have a smaller standard deviation than the 0-10% variations; however, the percent variations in the 10-50% burn angle are larger ($COV_{0\text{-}10\%}$=8.8% versus $COV_{10\text{-}50\%}$=12.7%) because the 10-50% burn angle is shorter than the 10-50%. Finally, the 50-90% burn angle has the widest distribution because of the influence of phasing; as the cycle progresses, slow cycles become even slower due to the poor combustion phasing.

Figure 2-11 shows the distribution of initial flame kernel convection velocity used as an input into the cycle simulation; the location of the ground electrode is shown for reference. The magnitude and direction distributions for these input data were scaled from fiber optic spark plug measurements made in the same engine at a higher speed operating condition [57]. As Figure 2-12 shows, the convection has very little effect on the early combustion, because the flame has not become large enough to interact with the combustion chamber geometry. For the 10-50% and the 50-90% burn angles, the distributions are somewhat wider, though still small compared with the actual variations observed in the engine test results. Holmström and Denbratt [48] and Shen et al., [49] found through similar quasi-dimensional modeling studies that variations in the flame interactions with the combustion chamber geometry had a small but significant influence on variations in the later portions of the combustion event.

Figure 2-15 shows the input distribution for residual mass fraction, and Figures 2-16 through 2-18 show the output burn duration distributions. The residual mass

variations appear to have a significant effect on combustion variations by influencing the laminar burning velocity.

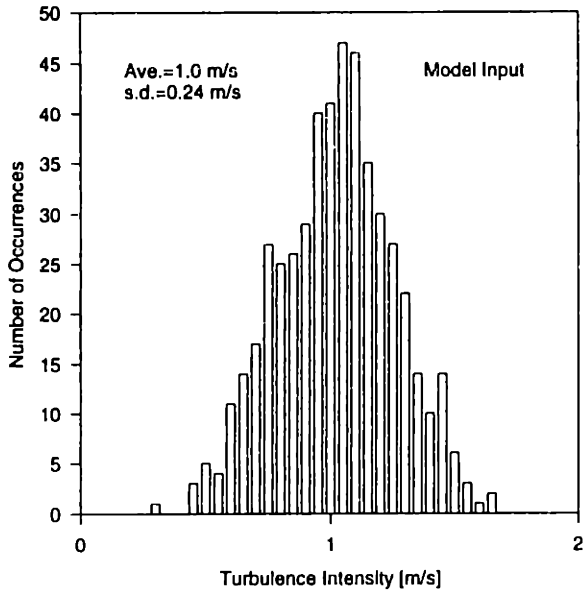


Figure 2-7. Test input distribution for u', 500 cycles.

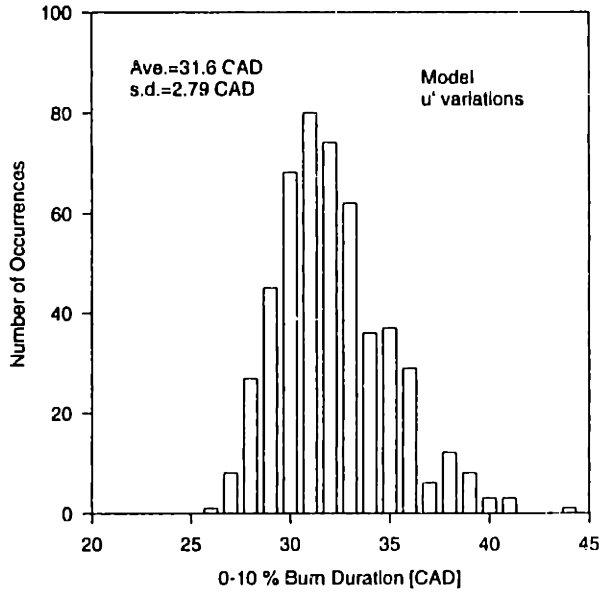


Figure 2-8. Distribution of 0-10% burn angle for variations in u', 500 cycles.

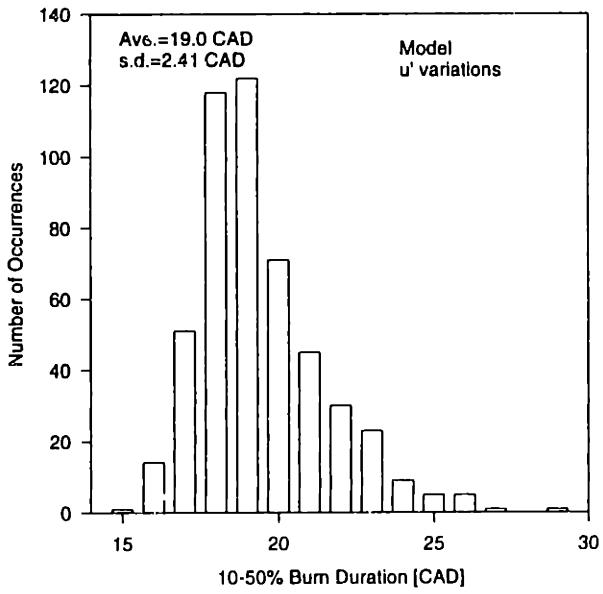


Figure 2-9. Distribution of 10-50% burn angle for variations in u', 500 cycles.

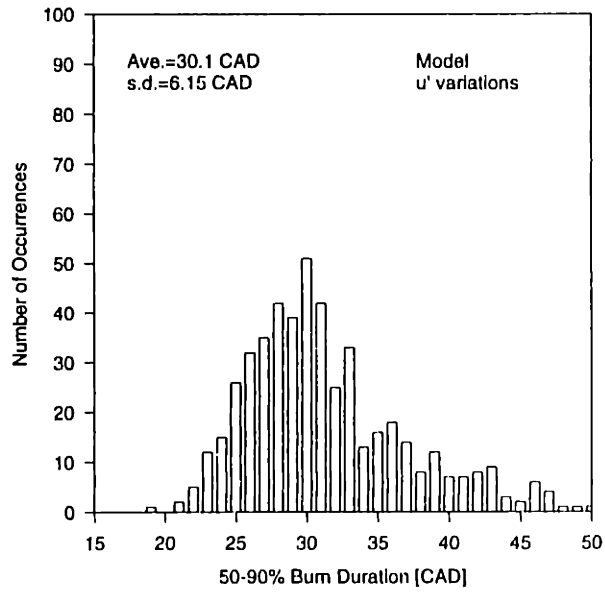


Figure 2-10. Distribution of 50-90% burn angle for variations in u'.

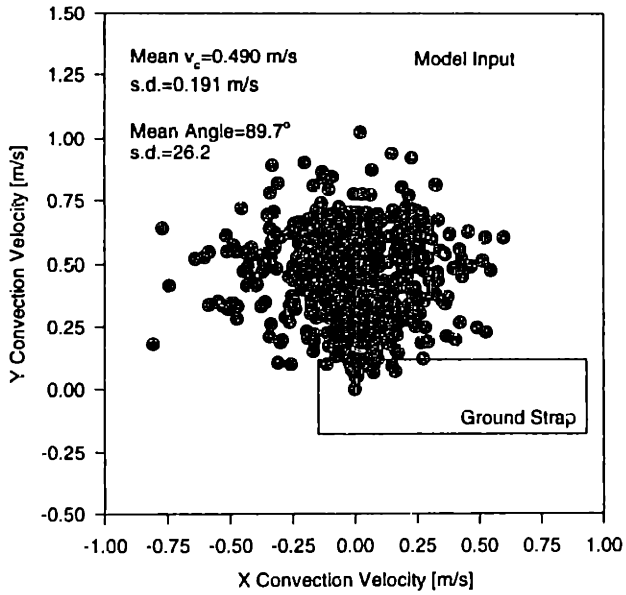


Figure 2-11. Test input distribution for initial kernel convection velocity.

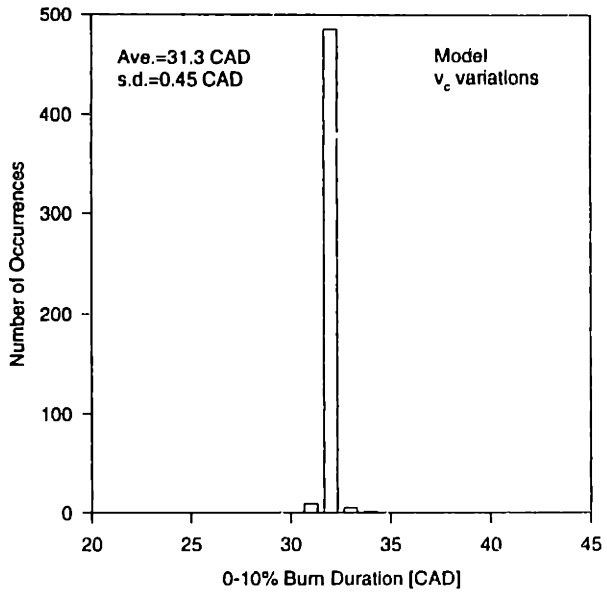


Figure 2-12. Distribution of 0-10% burn angle for variations in $v_c$, 500 cycles.

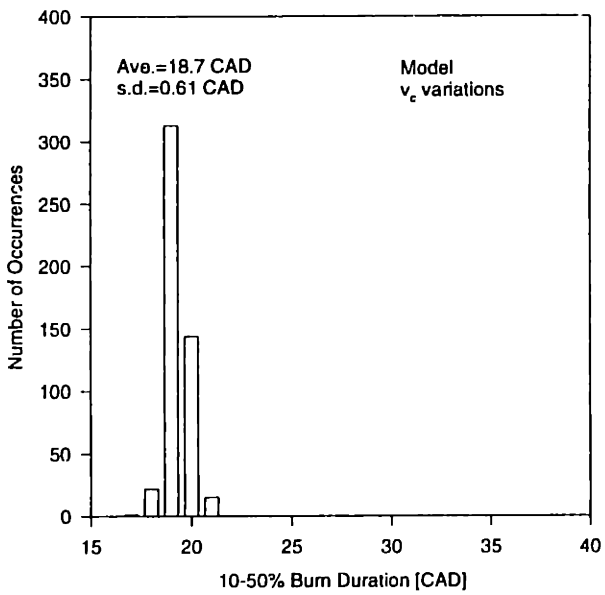


Figure 2-13. Distribution of 10-50% burn angle for variations in $v_c$, 500 cycles.

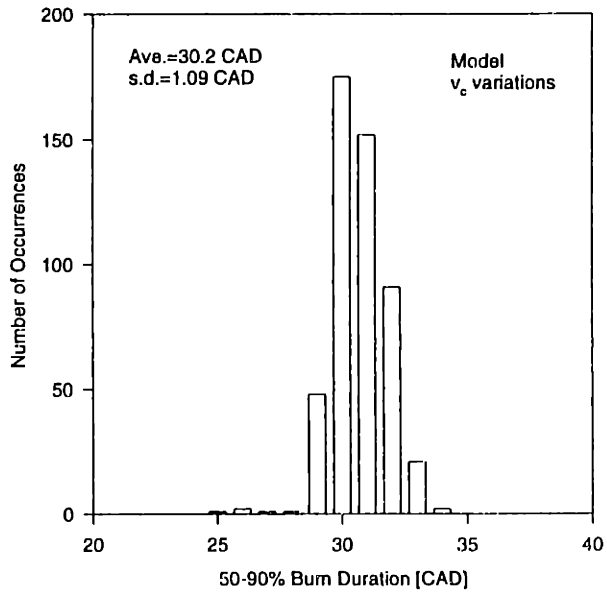


Figure 2-14. Distribution of 50-90% burn angle for variations in $v_c$, 500 cycles.

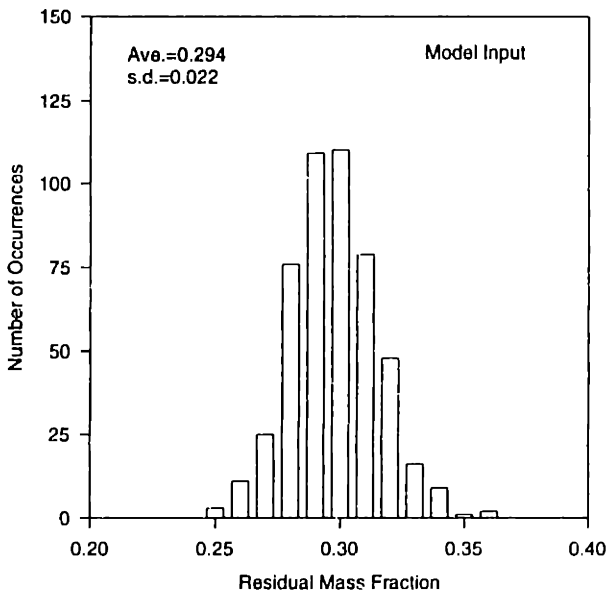


Figure 2-15. Test input distribution for residual gas fraction, 500 cycles.

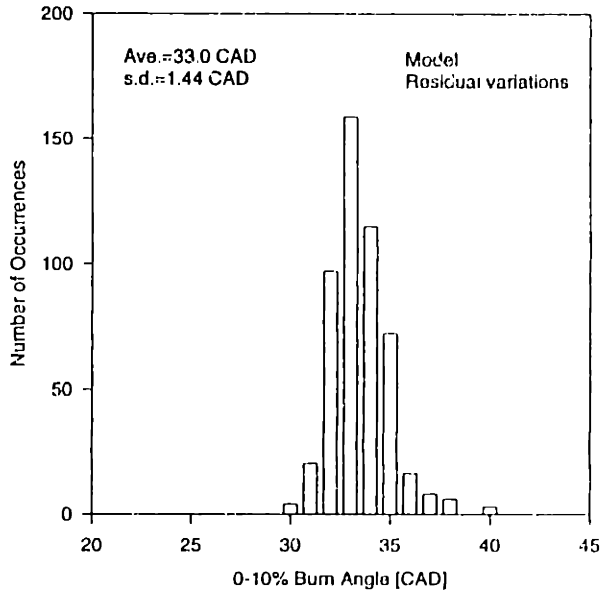


Figure 2-16. Distribution of 0-10% burn angle for variations in residual mass fraction, 500 cycles.

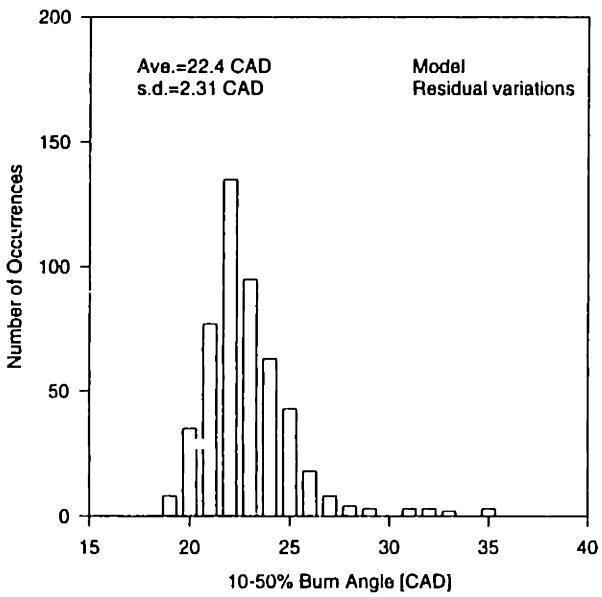


Figure 2-17. Distribution of 10-50% burn angle for variations in residual mass fraction, 500 cycles.

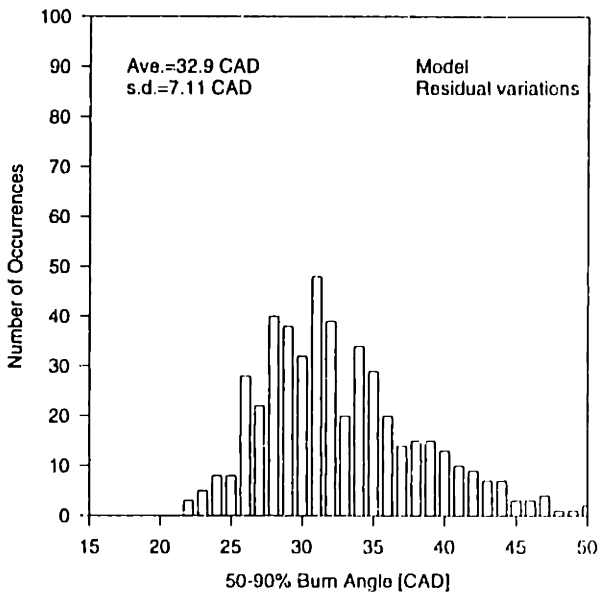


Figure 2-18. Distribution of 50-90% burn angle for variations in residual mass fraction, 500 cycles.

### 2.3.2. *SENSITIVITY RESULTS*

Investigating the influence of the input parameters on the cycle performance through cycle-to-cycle variation in the inputs is interesting from a qualitative standpoint, as it gives a "feel" for how each input influences the output. However, since the variations in the input parameters are not known, it is impossible to attribute the extent of output variations in an actual engine to each of the influencing parameters. Brehob and Newman [46] perturbed the inputs to a quasi-dimensional cycle simulation until they obtained output distributions that matched those of experiments; however, they limited their input variations to three parameters—initial kernel burn rate, displacement of the kernel from the spark gap, and turbulence intensity. If more influencing factors are included, there will be too many degrees of freedom, and parametric perturbation of the inputs will not give a unique answer.

One means of assessing the importance of an input parameter on the outputs is to consider the sensitivity: the amount of change in the inputs caused by a small perturbation in one of the inputs. Consider the case of two simulated engine cycles, identical in every respect, except the mass of fuel in one cycle is 5% higher than the other. This difference will result in changes in the combustion rate and the total amount of energy produced in the cycle. A sensitivity may be defined:

$$S^{x}_{y} = \frac{x}{y}\frac{\partial y}{\partial x} = \frac{\partial \ln y}{\partial \ln x}$$

where y is some output parameter, such as 10-50% burn time or IMEP, and x is the input parameter that was perturbed. The sensitivity, S, represents the influence that an input has on the combustion. A sensitivity higher than one means that a 1% change in the input will result in more than a 1% change in the output. The sensitivity may be calculated with the model by simulating two cycles that are the same except for a small perturbation in one input parameter. Figure 2-19 shows the modeled sensitivity results for perturbations in the charge composition and

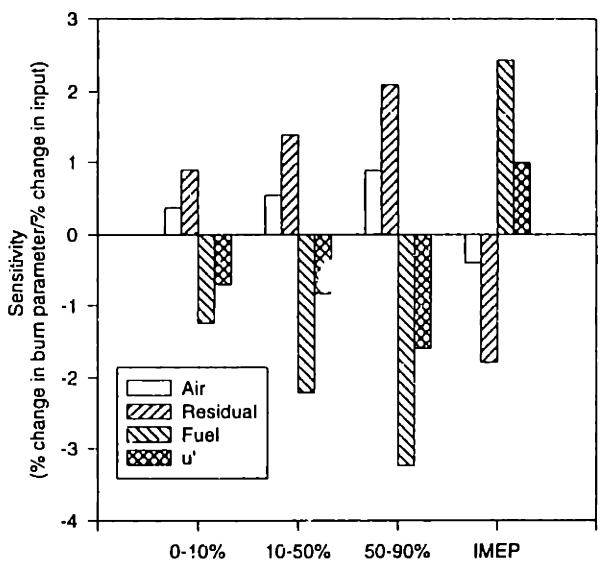


Figure 2-19. Comparison of simulation sensitivities for air, residual, fuel, and turbulence intensity.

turbulence intensity. Convection velocity was omitted from this graph because the sensitivity is negligible.

Figure 2-19 shows that the combustion is most sensitive to fuel mass, followed by residual, turbulence intensity, and air mass. In each case, the sensitivities are larger for the later burn angles; this is a result of phasing—slow cycles become slower, and fast cycles become faster relative to the mean. The sensitivity of IMEP to fuel mass is higher than one. If the engine were operating at MBT, one would expect that this value would be close to one; if 2% more fuel energy is added, there should be about 2% more energy extracted from the cycle.[8] This is because the mechanical energy output per cycle is relatively flat with respect to combustion phasing at MBT. However, since idle is significantly retarded with respect to MBT, any change in cycle phasing will have a large influence on the IMEP. Since an increase in fuel concentration results in an increase in laminar burning speed, there is a significant phasing benefit at the idle condition. In §6.2.3 a more thorough explanation of the reason for the relative differences in sensitivities is presented.

It should be stressed that Figure 2-19 is not the entire story. Without knowledge of the magnitude of the input variations (i.e., variations in $m_{residual}$, $m_{fuel}$, etc.), it is impossible to know how much each influencing factor contributes to cycle-to-cycle variability in combustion. That is to say, even though Figure 2-19 indicates that the combustion is more sensitive to a percentage change in fuel mass, if, in the

[8] Provided the perturbation experiment is kept lean of stoichiometric, as is the case in the perturbation used in this modeling study. A rich perturbation is more complex.

engine, the percent variation cycle to cycle in the residual mass is much higher than the percent variation in the fuel mass, the residual mass variations may contribute more to the overall cycle-to-cycle combustion variability.

# 3. EXPERIMENTAL APPROACH

## 3.1. Basis of Methodology

The objective of the experimental work is to develop a method whereby the variations of the engine "input" parameters (such as air mass, fuel mass, residual mass, etc.) could be deduced from the measurable engine output (such as IMEP, 0-10%, 10-50%, 50-90% mass fraction burn durations), The impetus for such a methodology was the result from Chapter 2, in which the engine system was modeled as a "black box" with various inputs and outputs. Variations in the inputs to the engine system resulted in variations in the outputs, and each input/output combination had an identifiable sensitivity that could be expressed as an equation of the following form:

$$S^{x_i}{}_{y_j} = \frac{\partial y_j}{\partial x_i} \qquad (3\text{-}1),$$

where S represents the sensitivity, $y_j$ is the output parameter, and $x_i$ is the input parameter. A distribution in the input variable x will result in a distribution in the output variable y; the spread and shape of the output distribution depends on the spread and shape of the input distribution *and* the sensitivity, $S^i_j$. This is

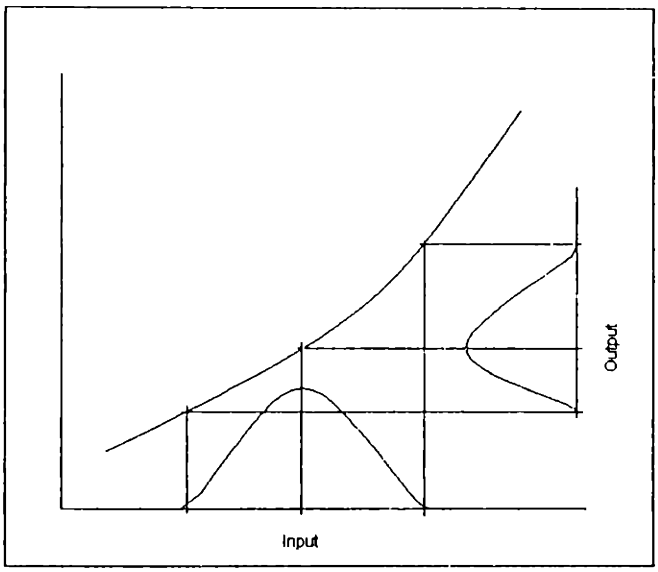


Figure 3-1. Example input distribution and resulting output distribution for an arbitrary sensitivity function.

represented graphically in Figure 3-1. The distribution on the horizontal axis represents the input dispersion, the slope of the curve is the sensitivity of the output parameter to changes in the input parameter, and the distribution on the right side is the resultant output spread. In this example, the sensitivity shown is not linear, resulting in a skewed output distribution from a symmetrical input distribution.

The important result from the modeling study was the observation that each input parameter had its own unique "footprint" that it left on the output parameters. Thus the system is well defined in the sense that information on the output parameters could be "inverted" to yield information on the input parameters. If the input deviations are assumed to be small, and the sensitivities may be approximated as linear, then one could write an equation to represent the influence of deviations in the various significant input parameters on a particular output parameter:

$$y_j - \bar{y}_j = \frac{\partial y_j}{\partial x_1}\delta x_1 + \frac{\partial y_j}{\partial x_2}\delta x_2 + \ldots + \frac{\partial y_j}{\partial x_i}\delta x_i \qquad (3\text{-}2).$$

The left side of this equation represents a deviation of the output parameter $y_j$ from the average value, $\bar{y}_j$, while the right side includes all of the small deviations of the input parameters from their average values, $\delta x_i$. The partial derivatives, $\frac{\partial y_j}{\partial x_i}$, are simply the sensitivities, $S^i_j$, as defined above in Equation 3-1. Since small perturbations were assumed, we may make the following substitution:

$$\left(\frac{\bar{x}_i}{\bar{y}_j}\frac{\partial y_j}{\partial x_i}\right) \equiv \frac{\partial\left(\ln y_j\right)}{\partial\left(\ln x_i\right)}$$

Rewriting Equation 3-2 as

$$\frac{\left(y_j - \bar{y}\right)}{\bar{y}_j} = \left(\frac{\bar{x}_1}{\bar{y}_j}\frac{\partial y_j}{\partial x_1}\frac{\delta x_1}{\bar{x}_1}\right) + \left(\frac{\bar{x}_2}{\bar{y}_j}\frac{\partial y_j}{\partial x_2}\frac{\delta x_2}{\bar{x}_2}\right) + \ldots + \left(\frac{\bar{x}_i}{\bar{y}_j}\frac{\partial y_j}{\partial x_i}\frac{\delta x_i}{\bar{x}_i}\right)$$

and making the above substitution yields the following equation:

$$\left(\frac{\delta y_j}{\bar{y}_j}\right) = \sum_i \left(\frac{\partial\left(\ln y_j\right)}{\partial\left(\ln x_i\right)}\right)\left(\frac{\delta x_i}{\bar{x}_i}\right) \qquad (3\text{-}3).$$

Thus, we have an expression for the relative fluctuations in the output parameters, $y_j$, as a function of the relative fluctuation in the inputs, $x_i$.

Equation 3-3 may be put in a more useful form if we make the assumption that the input fluctuations are independent of each other. Squaring both sides of Equation 3-3 yields

$$\left\langle\left(\frac{\delta y_j}{\bar{y}_j}\right)^2\right\rangle = \sum_i \left(\frac{\partial\left(\ln y_j\right)}{\partial\left(\ln x_i\right)}\right)^2 \left\langle\left(\frac{\delta x_i}{\bar{x}_i}\right)^2\right\rangle \qquad (3\text{-}4),$$

where the angle brackets indicate an aggregation. There are no cross-terms, because assuming the variations in $x_i$ are independent means that

$$\left\langle \delta x_i \delta x_k \right\rangle = 0 \qquad \text{where } (i \neq k).$$

The definition of the coefficient of variation (COV) is

$$COV_y = \frac{1}{\bar{y}}\sqrt{\frac{\sum_n \left(y - \bar{y}\right)^2}{(n-1)}}$$

where n is the number of samples. Using this definition, Equation 3-4 may be written as

$$\left(COV_{y_j}\right)^2 = \sum_i \left(\frac{\partial\left(\ln y_j\right)}{\partial\left(\ln x_i\right)}\right)^2 \left(COV_{x_i}\right)^2 \qquad (3\text{-}5).$$

To put it in a more compact form, let us make the following definitions:

$$\eta_j \equiv COV_{y_j}$$

$$\zeta_j \equiv COV_{x_j}$$

and

$$\mathbf{D}_{j,i} \equiv \sum_i \left(\frac{\partial\left(\ln y_j\right)}{\partial\left(\ln x_i\right)}\right)^2$$

Finally, Equation 3-5 may be written in matrix form as

$$\eta_j^2 = \mathbf{D}_{j,i}\zeta_i^2 \qquad (3\text{-}6).$$

Here, $\eta_j^2$ is a 4x1 column vector, $\zeta_i^2$ is a 3x1 column vector, and $D_{j,i}$ is a 4x3 matrix.

The vector $\eta_j^2$ is observable in engine experiments; it is simply a vector of the variations in the output parameters—$COV^2_{IMEP}$, $COV^2_{0\text{-}10\%\ burn\ angle}$, etc. Except through rather involved experiments (cf., §1.1.2), $\zeta_i^2$ is generally not observable. However, if the sensitivity matrix, $D_{j,i}$, were known, it would be possible to calculate the variations in the inputs, $\zeta_i^2$, provided that $j \geq i$, so that there are sufficient equations for the number of unknowns. For $j > i$, the system is overdetermined and may be found using the least-squares method.

## 3.2. Experimental Plan: Determining Cycle-to-Cycle Gas Composition Variations

### *3.2.1. CONSIDERATION FOR FACTORS THAT COULD NOT BE PERTURBED INDEPENDENTLY*

In the previous section, equations were developed that allowed the calculation of the fluctuations in the "input" phenomena from the observations of the "output" parameters, provided the individual sensitivities of the outputs to each of the inputs are known. The consequence of this observation is the possibility to determine the cycle-to-cycle fluctuations of important variability-causing parameters, such as residual mass fraction. The sensitivities for fuel mass, residual mass, air mass, and turbulence intensity were calculated using a computer model of an engine cycle in Chapter 2. However, because of the uncertainties in the model, those results were for illustrative purposes only; it would not be accurate to apply the calculated sensitivities to actual engine experiments. What is necessary is an *experimental* determination of the relevant sensitivities on an engine.

The means by which the sensitivities are determined on an engine is analogous to the method used in the simulation: a small perturbation in an input parameter will result in an observable deviation in the outputs. However, it is not possible to perform this sort of perturbation experiment for all of the important input phenomena that are thought to contribute to cyclic combustion variability. In particular, the flow factors—turbulence and bulk gas flow—represent a problem. On the other hand, charge composition variables may be perturbed in this manner; details on a methodology for determining gas composition sensitivities in an engine will be presented in the next section.

The analysis from §3.1 required that the sensitivities be known for all of the relevant inputs. Since it is only possible to experimentally determine gas composition sensitivities, this analysis needs to be modified somewhat. Consider Equation 3-2 in terms of the gas composition variables:

$$y_j - \bar{y}_j = \frac{\partial y_j}{\partial m_a}\delta m_a + \frac{\partial y_j}{\partial m_f}\delta m_f + \frac{\partial y_j}{\partial m_r}\delta m_r + [others]_j$$

where $m_a$ is total air mass in the charge, $m_f$ is fuel mass, and $m_r$ is residual mass. The "[others]" term is a catch-all that is used to represent all of the other important phenomena that influence cycle-to-cycle variations for which the sensitivities cannot be determined experimentally. The presence of the "[others]" term does not invalidate any of the previous analysis, so that Equation 3-6 may be rewritten as

$$\eta_j^2 = \mathbf{D}_{j,i}\zeta_i^2 + [others]_j \qquad (3\text{-}7)$$

where the indices i of value 1 through 3 refer to the mass of air, fuel, and residual respectively. Values of 1-4 have been used for the index j; specifically, they represent the 0-10%, 10-50%, and 50-90% mass fraction burn durations and the IMEP. Thus, Equation 3-7 designates an overdetermined set of equations from which a least-squares solution may be determined. The output parameters that are used for the vector $\eta$ will be further discussed in §5.26.1.

In Equation 3-7, the left side is know by observation of engine data and the matrix $D_{j,i}$ may be determined through gas perturbation experiments. All that remains in order to solve for the input variations, $\zeta_i^2$, is to get rid of the "[others]" term. This may be achieved by performing a set of skip-fired experiments with controlled composition to eliminate cycle-to-cycle variations in the masses of air, fuel, and residual. For details on the skip-firing experiments, refer to §3.2.2.1. In the case of such a "baseline" experiment, the only source of cycle-to-cycle variations in the measured output parameters would be the "[others]" term. In the form of an equation,

$$\eta_{j,0}^2 = [others]_j$$

where $\eta_{j,0}^2$ is the observed output variation from the skip-fired experiment.

Now, Equation 3-6 may be written as the following:

$$\left(\eta_j^2 - \eta_{j,0}^2\right) = \mathbf{D}_{j,i}\zeta_i^2 \qquad (3\text{-}8)$$

Using least-squares, it is possible to find a solution for $\zeta_i^2$

$$\zeta_i^2 = \left[\left(\mathbf{D}^T\mathbf{D}\right)^{-1}\mathbf{D}^T\right]\left[\left(\eta_j^2\right) - \left(\eta_{j,0}^2\right)\right] \qquad (3\text{-}9).$$

This is our desired answer; by multiplying the appropriate sensitivities by the variations in the inputs, we may determine the relative contribution of variations in air, fuel and residual mass to the overall cycle-to-cycle combustion variability.

### *3.2.2. EXPERIMENTS*

#### 3.2.2.1. Skip-Firing Experiments

The analysis of the previous sections developed a means whereby the influence of variations in the gas composition on cycle-to-cycle combustion variations may be determined. Because the influence of other factors—such as turbulence variations—may not be ignored, it is necessary to perform "baseline" experiments in which there are no cycle-to-cycle variations in the charge composition. This objective may be achieved through pre-mixing the charge well upstream of the inlet and skip-firing the engine. The methodology of such an experiment is described in detail by Sztenderowicz [37]; his description will be summarized here.

In ordinary operation, cycle-to-cycle variations in the charge composition are a consequence of many factors (cf. §1.1.2.2): shot-to-shot variations in the injected fuel amount, variations in the burned gas density resulting in variations in the residual fraction, etc. Such variations are impossible to eliminate entirely in a port-fueled, continuously fired engine; however, by prevaporizing the fuel and mixing it with air well upstream of the engine inlet, variations in the equivalence ratio may be eliminated. Also, if the engine were not fired every cycle, the variations in residual gas mass may be eliminated as well. By skipping enough cycles in between the fired cycles, the residual from the last fired cycle would be completely purged before the next fired cycle. The number of cycles that must be skipped to completely

eliminate the residual depends on the purge rate of the engine at the specified operating condition.

Since the process of skip-firing eliminates the natural residual present in the engine, and since the skip-firing experiments are meant to simulate ordinary continuously-fired operation, it becomes necessary to supply to the engine, along with the fuel and air, an amount of artificial residual that matches the amount of actual residual under ordinary operation. The artificial residual is a mixture of $CO_2$ and $N_2$ that matches the molar heat capacity of the actual residual gas; the method of determining the exact composition of the artificial residual is described in Appendix A. To perform the skip-fired experiments, it is necessary to determine the average amount of natural residual in the cylinder at the operating condition to be matched in the skip-fire experiments; the procedure and results for this are described in §4.2.4. Details of the implementation of the skip-firing experiments are reported in §5.3.

### 3.2.2.2. In-Cylinder Composition Perturbation Experiments

The methodology for determining the sensitivity matrix, $D_{j,i}$, described in §3.1 is similar in principle to the modeling study of Chapter 2. The charge composition is perturbed on a cycle-to-cycle basis by adding a small amount of air, fuel, or residual. The influence of this perturbation on the engine performance is then determined by analyzing the cylinder pressure data and comparing perturbed and non-perturbed cycles. Figure 3-2 shows a representation of the method for residual gas injection.

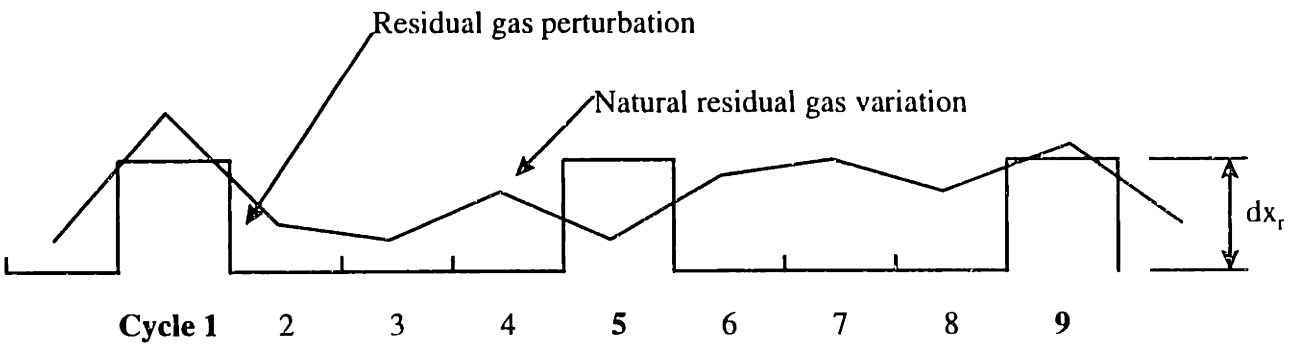


Figure 3-2. Synchronized detection of parameters: residual gas perturbation.

In this figure, the ordinary cycle-to-cycle fluctuation of the residual gas in the cylinder is represented by the wavy line, and the perturbation of the residual fraction, $dx_r$, is represented by the square pulse every fourth cycle; the total residual mass in the cylinder is a superposition of the natural variation and the perturbation. By sampling over many cycles and comparing the combustion characteristics of the perturbed cycles with the non-perturbed cycles, the sensitivity of the combustion to variations in residual mass may be determined. The same experiments may be performed for air and fuel perturbations. For small enough perturbations in composition the sensitivities will be linear; however, there is no way of knowing *a priori* how small is "small enough." Thus, to ensure that the measured sensitivity is linear, experiments with two different amplitudes of perturbation are performed, and the sensitivities are compared. The details of the implementation of the perturbation experiments are described in §5.2.

# 4. Engine Setup: Description and Characterization of Idle Operation

## 4.1. Engine Setup

### *4.1.1. The Nissan SR20DE*

Table 4-1 shows the relevant characteristics of the engine used in the experimental portion of this work. The SR20DE has a pentroof head with a centrally-located spark plug. Although no measurements were made, the configuration and symmetry of the intake ports suggest that there is no significant swirl present in the cylinder. Measurements with a fiber optic spark plug probe from a previous work indicate that there is an observable tumble motion in the chamber [57]; this observation is consistent with the intake port configuration and the pentroof shape of the head.

The engine was modified to operate on a single cylinder to avoid

Table 4-1. Nissan SR20DE specifications.

| | |
|---|---|
| Engine Type | 4 cylinder, 4 valve/cylinder DOC Aluminum head/block |
| Bore x Stroke [cm] | 8.6 x 8.6 |
| Compression Ratio | 9.5 |
| Displacement/cylinder [$cm^3$] | 499.6 |
| Clearance volume/cylinder [$cm^3$] | 58.77 |
| Intake valve (34 mm diameter) | Open 527° ABCC<br>Close 55° ABCC |
| Exhaust valve (30 mm diameter) | Open 303° ABCC<br>Close 543° ABCC |
| Valve overlap | 16° |

multiple cylinder interactions. Thus, fuel is injected and a spark is supplied to only one cylinder (the number 4 cylinder), and the intake and exhaust runners of the firing cylinder are isolated. No modifications were made in the moving parts to preserve the inertial balance of the engine.

The engine was coupled to a Dynamatic dynamometer, which may be used to turn the engine while motoring or absorb power when the engine is firing. One consequence of firing the engine with only one cylinder is that the dynamometer must turn the engine at low loads because the power produced by a single cylinder is not enough to overcome the friction of the engine. The dynamometer, controlled by a Digalog controller, was thus used to turn the engine at a constant speed of 800 RPM for all experiments. Though instantaneous engine speed was not recorded, preliminary measurements indicated that speed fluctuations were generally held below 0.5% at the chosen idle operating condition. This method of engine speed control, while not typical of idle in an automobile, was a constraint of the engine/dynamometer system and could not be helped.

The engine coolant system was modified to include a water heater; this allowed the engine coolant temperature to be maintained at a temperature around 80° C for all tests. The heater also allowed preheating of the engine block and head, greatly reducing the amount of warm-up time required before data could be taken. An oil cooling circuit controlled the temperature of the oil in the sump, which was kept at approximately 75° C for all experiments. The temperatures of the inlet air and exhaust port were also recorded for each experiment.

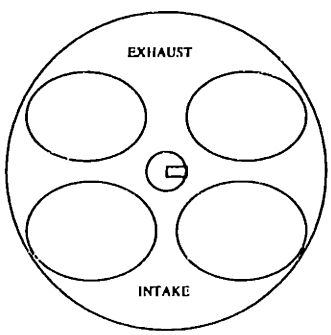


Figure 4-1. Spark plug orientation used for all experiments.

The spark plug ground electrode orientation was kept constant for all experiments. Spark plug location and orientation are shown in Figure 4-1. The plug used was a NGK BKR7E, with a plug gap of 0.9 mm, as

specified by the manufacturer. The spark energy deposited was 50mJ.

### *4.1.2. GAS SUPPLY AND PREPARATION*

The engine air supply was regulated by Tylan General mass flow controller model FC 262, with Tylan readout/control box model RO-28. For the set of skip firing experiments described in §5.3, several important additions to the engine gas supply system needed to be made. Figure 4-2 shows a schematic of the gas supply/mixture preparation system used for all experiments. In order to match ordinary operation in the skip-firing experiments, artificial residual ($N_2$ and $CO_2$—see Appendix A) needed to be supplied along with the air and fuel. These gases were metered to the gas supply manifold via critical flow orifices, which allowed precise mass flow control regardless of the inlet manifold pressure. Also, the inlet air and artificial residual were heated so that the temperature of the charge at time of spark in the skip-firing experiments matched ordinary operation. The location of the heating element is shown in Figure 4-2. A perforated plate was placed upstream of the engine inlet manifold to provide adequate mixing of the charge.

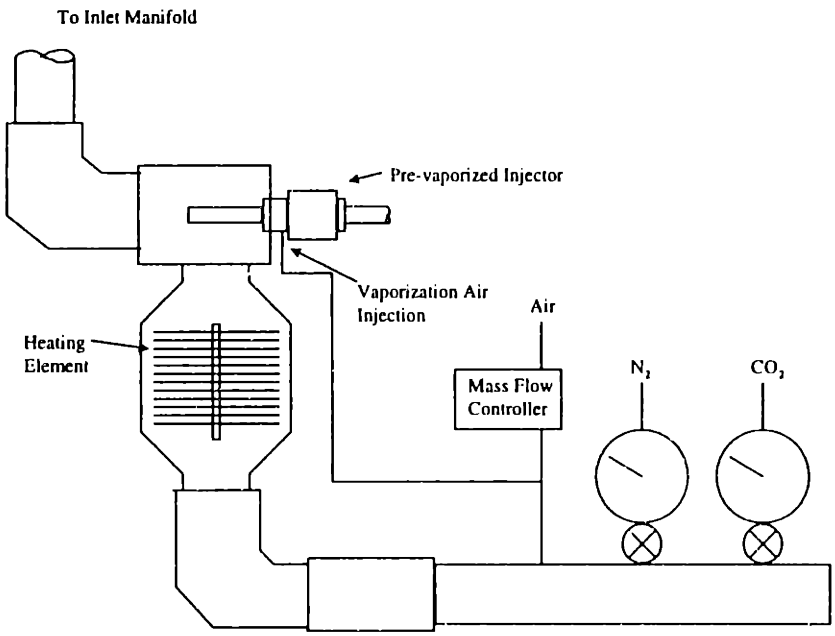


Figure 4-2. Schematic of mixture preparation apparatus.

### *4.1.3. FUEL PREPARATION METHODS*

The Nissan SR20DE ordinarily operates with an electronic multi-point port fuel injection system. The standard injectors are of the four-hole spray collision type, with dual direction injection; the injector targeting is on the back of the inlet valves, with minimal wall flow resulting from the dual direction aiming. The original injector controller for the engine was replaced with a separate controller that timed injection at a constant crank angle each cycle; in these experiments, the timing of the injection was kept at 100° after bottom center compression, on a closed intake valve. While injection timing was referenced by crank angle, injection duration was controlled in units of milliseconds, making injection amount controllable independent of engine speed. In all experiments, except for the residual gas measurements described below, indolene was the fuel used. Figure 1-1 shows the amount of indolene injected as a function of pulsewidth for the stock Nissan injector.

In §4.2.4, experiments for measuring the average residual gas content are described. For these experiments the engine was fired with propane as the fuel since liquid fuel would interfere with the in-cylinder gas sampling and analysis. The propane was introduced into the intake runner, approximately 30 cm upstream of the inlet valves; the flow rate was controlled by a needle valve. Pressure data analysis for propane operation showed cycle-to-cycle variability comparable to operation with port fuel injection, indicating that there was adequate mixing between the air and fuel introduced in this manner.

Finally, for experiments where a perfectly homogeneous charge was required, the standard port fuel injection was disabled, and a prevaporized injection system obtained from the National Engineering Laboratory of UK was employed; the system is described by Fox et al. [58]. The prevaporized injector apparatus consisted of a Bosch model # 0-280-150-151 injector in a machined housing with three air jets; two air jets were aimed into the flow tangentially, and the third was aimed radially. The injected fuel and air pass down a 6 cm length of ¼" NPT brass

tubing, which is heated by a strap heater. The fuel impinges on the hot wall of the tube and vaporizes, and the swirling air flow entrains the vapor and mixes with the primary air flow. The injected air flow is estimated to be on the order of 40% of the total air flow required to operate the engine at idle. A thermocouple at the end of the tubing is used to control the temperature to be approximately 110° C, which was determined to be an appropriate temperature for complete vaporization of indolene fuel.

For all experiments, the air-fuel ratio was monitored with a Horiba AFR Analyzer (Mexa-110λ) oxygen sensor.

### *4.1.4. CYLINDER PRESSURE MEASUREMENT*

Cylinder pressure was recorded with a flush-mounted Kistler 6051B piezoelectric pressure transducer mounted in the cylinder head approximately 1 cm above the cylinder block. The transducer was connected to a Kistler model 5004 dual mode charge amplifier. The voltage output of the amplifier was sampled by a pc-based digital data acquisition system using a Data Translation A/D card (model DT2828). Pressure data were taken at a 1° interval using the pulse from a 360 pulse/revolution optical shaft encoder as an external trigger. The shaft encoder also provided a reference pulse at bottom center.

Since piezoelectric pressure transducers do not provide an absolute measurement of pressure, it was necessary to "peg" the transducer—i.e., reference the transducer output to an absolute pressure measurement—with a manifold pressure sensor (Data Instruments model SA). Randolph [59] determined that, for untuned intake systems and tuned systems at low speeds, pegging at bottom center before compression provided good accuracy. Thus, the pegging method chosen for this study was to average the voltage value of the first five pressure data points acquired after BC before the compression stroke and reference this average voltage to the pressure measured by the inlet manifold pressure sensor.

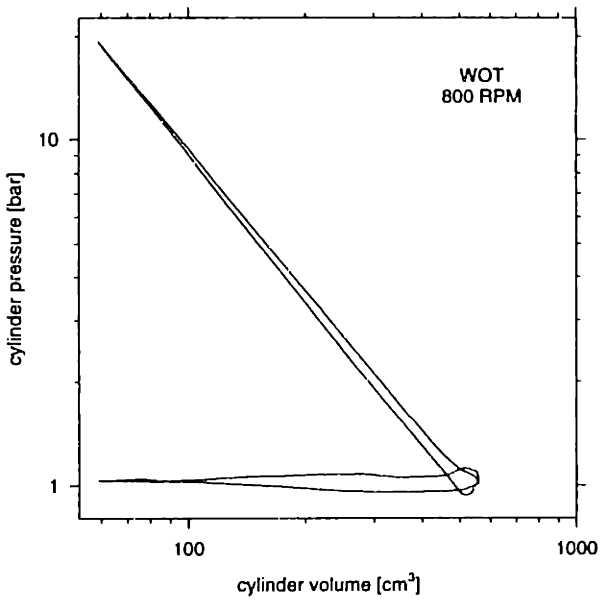


Figure 4-3. Log P vs. Log V plot of motored pressure data at wide open throttle.

Many studies have addressed the topic of in-cylinder pressure data accuracy [60, 61, 62]. Lancaster et al., [60] stress the diagnostic importance of a logarithmic plot of pressure versus volume data for a motored engine. Figure 4-3 shows such a plot for the apparatus used in this study. The linearity of the compression and expansion stroke, as well as the sharpness of the point at which they meet, indicate that the pressure data are correctly phased with respect to volume. The compression polytropic constant is 1.35, and the expansion polytropic constant is 1.42; these numbers are well within the desired range for motored data.

Accuracy of the pegging process may also be determined through examination of the motored pressure trace. Figure 4-4 shows a logarithmic plot of pressure versus volume for an average motored pressure trace with the inlet manifold pressure at 0.32 bar; this is the inlet pressure used for the experimental condition of this study. Curvature in the compression and expansion lines in this plot would indicate inaccurate pegging; however,

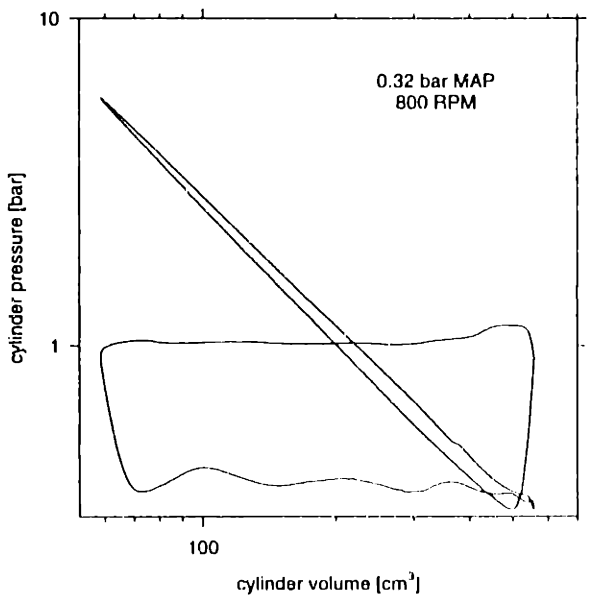


Figure 4-4. Log P vs. Log V plot of pressure data with MAP=0.32 bar.

the compression and expansion strokes are both very linear.

## 4.2. Characterization of the Idle Operating Condition

### *4.2.1. Operating Condition Selection*

As mentioned in §4.1, the engine control system for the Nissan has been replaced with individually adjustable controls for spark timing, fueling, etc. This fact, as well as the many modifications that were made to the engine, makes it impossible to let the engine idle as it would in a vehicle. Thus, it was necessary to find an appropriate idle condition; Table 4-2 shows the operating condition selected. The spark timing and speed were selected to be the values specified by Nissan for the idle condition of the engine. The air/fuel equivalence ratio, $\lambda$, was kept at a value of 1.0 because the engine normally operates with a three-way catalyst, and so stoichiometric operation is a constraint of the system. The inlet manifold pressure was adjusted to give an average gross IMEP of 1.55 bars, which is a value typical of an idle condition. All experiments were performed with the engine at a fully warmed-up state.

Table 4-2. The idle operating condition.

| | |
|---|---|
| Engine speed [RPM] | 800 |
| Inlet manifold pressure [bar] | 0.32 |
| Spark timing [CAD BTC] | 15° |
| Air/fuel equivalence ratio | 1.0 |
| Air mass flow rate [g/s] | 0.60 |
| Gross IMEP [bar] | 1.55 |

### *4.2.2. Characteristics of Idle Operation*

Figure 4-5 shows firing data of four consecutive cycles for the Nissan idle operating condition. These cycles are typical of idle, and may be used to demonstrate some of the features of idle operation. One characteristic that is immediately obvious is that there is quite a large difference between the pressure development of these cycles; this variability in the pressure is the result of variations in the combustion. For comparison, Figure 4-6 shows the burn rate profiles obtained through analysis of the pressure data with a burn rate analysis

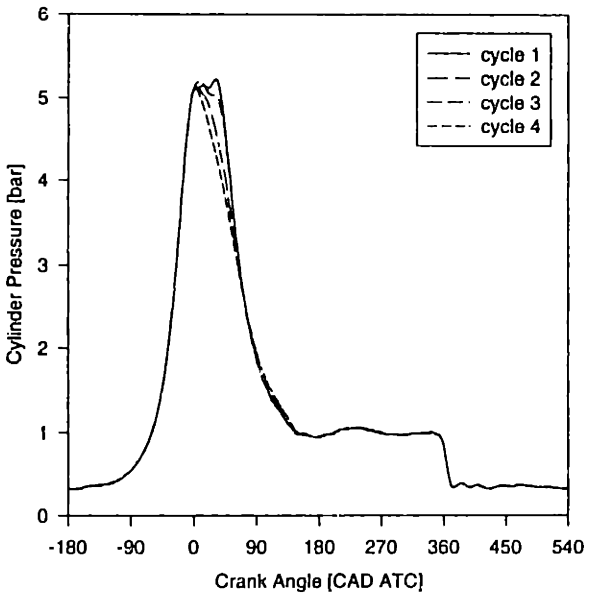


Figure 4-5. Pressure traces of four consecutive cycles at idle.

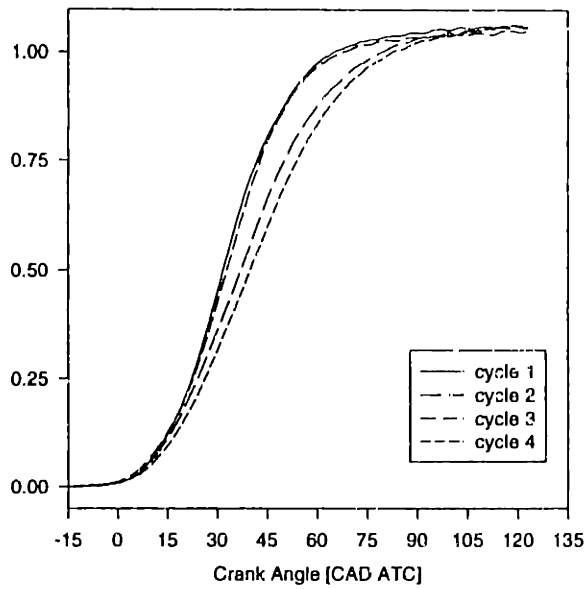


Figure 4-6. Burn rate profiles of four consecutive cycles at idle.

program. The peak pressures for cycles 2 and 4 are very close to top center, while cycles 1 and 3 show a "double-hump" in the pressure trace near the peak. The compression stroke, from 180° BTC until TC, is very repeatable, as is the exhaust pressure.

Side to side comparison between the burn rate profiles and the pressure traces also yields some interesting observations. Cycles 2 and 4 are noticeably slower than cycles 1 and 3, a fact that is obvious from the pressure traces. Cycle 3 initially has the fastest burn rate, though cycle 1 passes it at approximately 10% mass fraction burned; this is why cycle 3 has a higher peak pressure than cycle 1 near TC, but then cycle 1, after a slight dip in pressure, ends up having the highest peak overall. Later in the cycle—at about 50° ATC—the burn profile of cycle 3 "catches up" to cycle 1, but then cycle 1 speeds up once again. While cycles 2 and 4 are significantly slower than cycles 1 and 3, by the time the exhaust valve opens, all of the cycles appear to reach very similar final mass fractions burned. The burn rate profiles clearly indicate that the various stages of the burning process, as well as the total amount of mass burned, are dependent on different factors; thus, a cycle

that starts off burning very quickly may slow down in the later burn stages, or vice-versa.

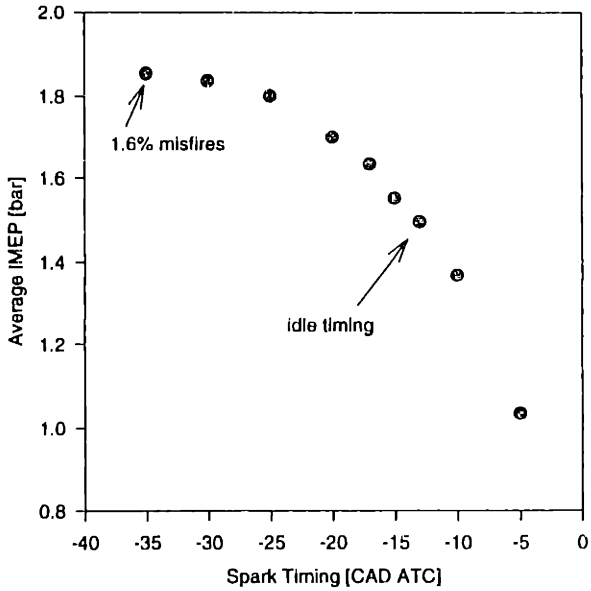


Figure 4-7. Spark map for 800 RPM, 0.32 bar inlet pressure.

As mentioned in Chapter 1, the spark timing at idle is significantly retarded from the optimum timing. Figure 4-7 shows a spark map at the same speed and inlet pressure condition as idle. The only occurrence of misfires was in the most advanced case (35° BTC spark); there were partial burns in the 35° case and the 5° case.[9] The misfired cycles and partial burns were eliminated for calculation of the average. This figure shows that optimum timing—provided there were no misfired cycles—is well advanced from the idle timing. From Figure 4-7, MBT would appear to be at 35° BTC or earlier; however, the presence of misfires prevents this spark timing from being practical. This is a common problem at low load: the low in-cylinder temperatures hinder ignition. Since in-cylinder pressure, and therefore temperature, is lower for more advanced timing, the occurrence of misfires increases as spark is advanced. Figure 4-7 shows that IMEP is quite sensitive to phasing changes at idle timing, whereas close to MBT the curve becomes flat. Thus, relative changes in combustion phasing have a larger influence on IMEP at idle because of this high sensitivity.

Perhaps the most accurate way of determining how retarded a particular condition is with respect to MBT is by calculation of the location of the 50% mass fraction burned point [63]. Figure 4-8 shows the data for this parameter for the spark sweep. According to reference [63], for MBT timing, the 50% point occurs at

[9] For the purposes of the pressure data analysis, misfires are identified as those cycles that have a gross IMEP of less than zero. The definition of a partial burn is a cycle with a gross IMEP that is between zero and one half of the mean IMEP of the sample.

approximately 7° ATC, and the distance of the 50% point for a particular condition from 7° ATC may be taken as a direct measurement of how retarded the condition is from MBT. This figure clearly shows that even the most advanced timing is quite retarded with respect to optimum.

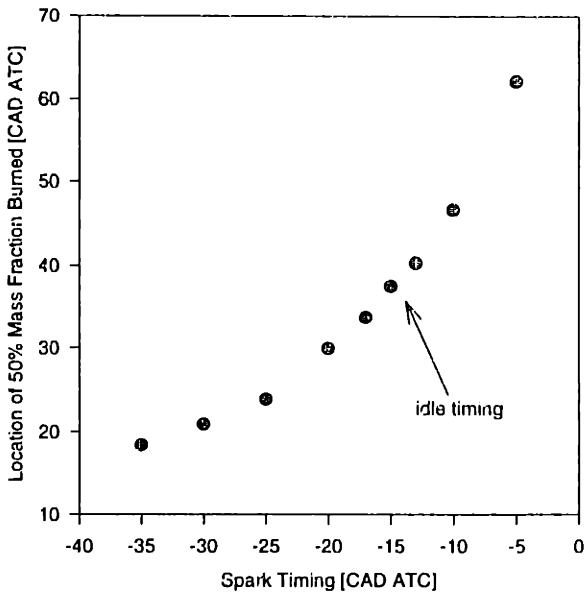


Figure 4-8. Location of 50% mass burned fraction vs. spark timing.

### *4.2.3. COMBUSTION VARIATIONS AT IDLE*

While four cycles may be sufficient to show that significant cycle-to-cycle combustion variability exists, statistical analysis of many cycles is required to describe the characteristics of that variability. It was stated in §1.1 that engine designers need to be concerned with engine torque fluctuations, as this is what the driver feels. However, instantaneous torque is a less convenient and informative measurement to make than cycle averaged properties. Amann [61] found that cycle-to-cycle variations in IMEP correlate well with instantaneous torque variations, making IMEP an appropriate parameter to characterize the variability of an engine.

A statistic that is typically used to characterize cycle-to-cycle variability is the coefficient of variation:

$$COV_y = \frac{1}{\bar{y}}\sqrt{\frac{\sum_n (y-\bar{y})^2}{(n-1)}}$$

where n is the number of samples and $\bar{y}$ is the average value of the sample. COV is the standard deviation (SD) of a sample, divided by the mean value of the sample. Hoard and Rehagen [44] explain why $SD_{IMEP}$ is preferable to $COV_{IMEP}$ when considering combustion variability, since the magnitude of the variation is what is

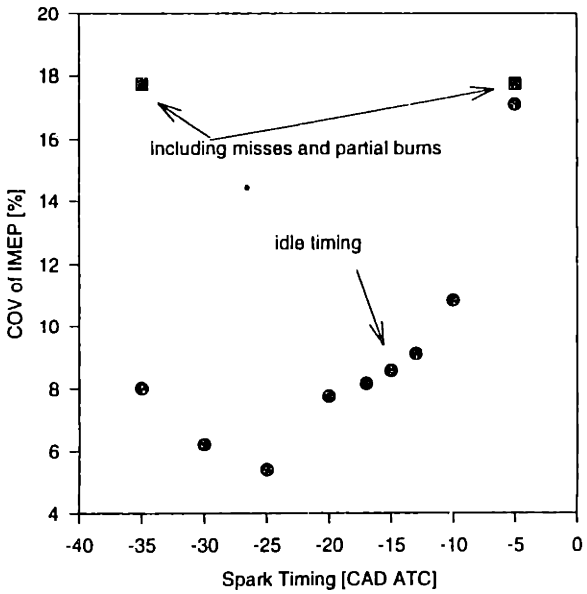


Figure 4-9. COV of IMEP for spark sweep.

perceptible and not the percentage variation from the mean; however, they also note that, since the mean value of IMEP is constant at idle, there is no statistical differentiation between COV and SD. In this study, COV will be used because it is more convenient for the analysis described in Chapter 3.

Figure 4-9 shows the influence of combustion phasing on the COV of IMEP. As the spark is advanced, the COV goes down because relative changes in combustion phasing have a smaller effect on the IMEP, as the spark map indicated. However, for the two most advanced cases, the COV begins to increase again, probably because the lower temperature at the time of spark is adversely affecting the ignition. Note that the COV of IMEP at the idle spark timing is slightly under 10%, which is typically considered the limiting point above which combustion variability is unacceptably high [23].

Hoard and Rehagen [44] propose one other means of characterizing cycle-to-cycle variations: the Lowest Normalized Value (LNV). The purpose of this parameter is to assess the misfire tendency of an engine; tests have shown that LNV correlates well with drivers' subjective rating of engine smoothness. Hoard and Rehagen define LNV as

$$LNV(\%) = \frac{100 \times (IMEP_{min})}{\overline{IMEP}}$$

where $IMEP_{min}$ is the minimum IMEP value in the data set, and $\overline{IMEP}$ is the mean IMEP of the data set. This value is plotted for the spark sweep in Figure 4-10. Hoard and Rehagen suggest that an appropriate acceptable value for the lower limit of LNV would be 75%. As the figure shows, the Nissan only matches that criterion at the 25° BTC spark timing.

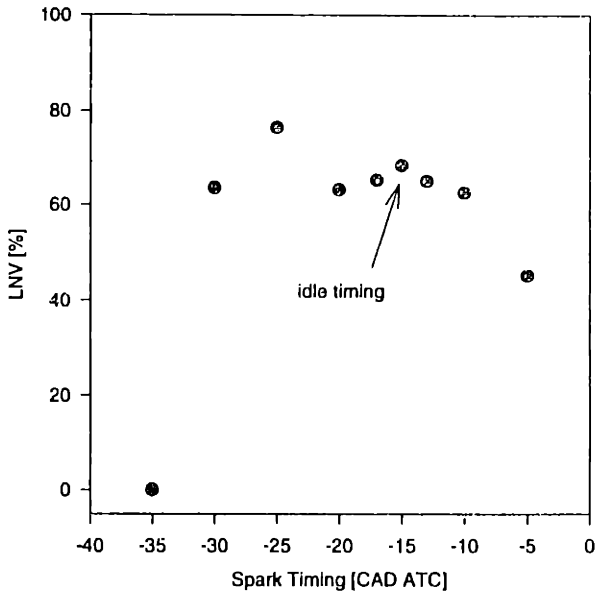


Figure 4-10. Lowest normalized value for spark sweep.

### *4.2.4. Determination of the Residual Fraction at Idle*

The experimental methodology described in Chapter 3 requires that the exact charge composition be known at the idle condition so that it is possible to match skip fired experiments to continuous firing. Figure 4-11 shows a schematic of the apparatus used to measure the average

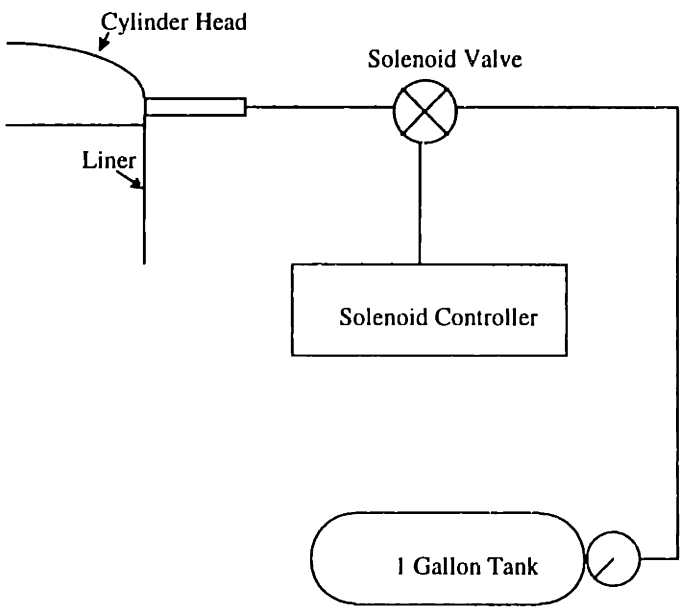


Figure 4-11. Schematic of apparatus for measuring in-cylinder residual gas concentration.

residual fraction in the Nissan engine. A sampling tube (ID = 0.15 mm) was mounted in a blank that fit into the pressure transducer mounting hole. This was connected to an evacuated 1 gallon tank via a fast-response solenoid valve (Kip, Inc. model # 141110). The engine was fired with propane because condensation of liquid fuel would interfere with the sampling apparatus.

It was necessary to disable the spark during sampling to allow enough time for an adequate amount of gas to be taken. Every seventh cycle the spark was disabled and a sample was taken by opening the solenoid valve for a period of 25 milliseconds. Seven cycles was chosen on the basis of preliminary tests to determine how long it would take for the engine to recover from a missed cycle; no difference was found between skipping five cycles and skipping seven cycles, so seven cycles was chosen to be conservative. Because it was important that the solenoid valve closed before the exhaust valve opened, the sampling duration of 25 milliseconds was chosen to allow for a 15 millisecond lag between the end of the sample pulse and solenoid valve closing.

Sufficient samples were taken to fill the evacuated tank to 6 psia (~ 2000 sampled cycles), and then the tank was pressurized with nitrogen up to 30 psia. Pressurizing the tank was necessary for gas analysis. The gas was tested for $CO_2$ content with a Rosemount infrared $CO_2$ analyzer (3% full scale). A spark sweep at the idle operating condition was performed; results for the average residual mass fraction are shown in Figure 4-12. The error bars represent the limit of the scale resolution for the $CO_2$ analyzer. This graph shows that the average residual content of the charge increases as the spark is advanced; the reason for this may be seen in Figure 4-13, which shows the temperature taken by a thermocouple at the exhaust port. The exhaust temperature goes up as the timing is retarded because more fuel energy is available due to the late phasing. As the exhaust temperature goes up, the residual gas density goes down, and thus there is less residual in the charge. The residual content of the charge at the idle spark timing is 27.4% by mass.

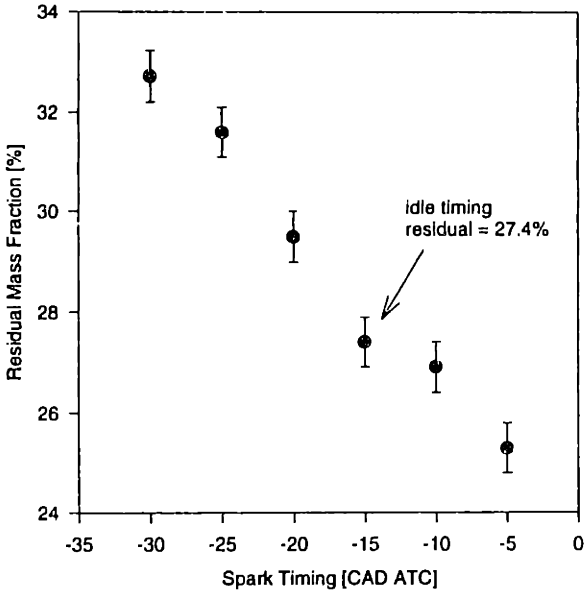


Figure 4-12. Residual gas fraction at 800 RPM and 0.32 bar inlet pressure.

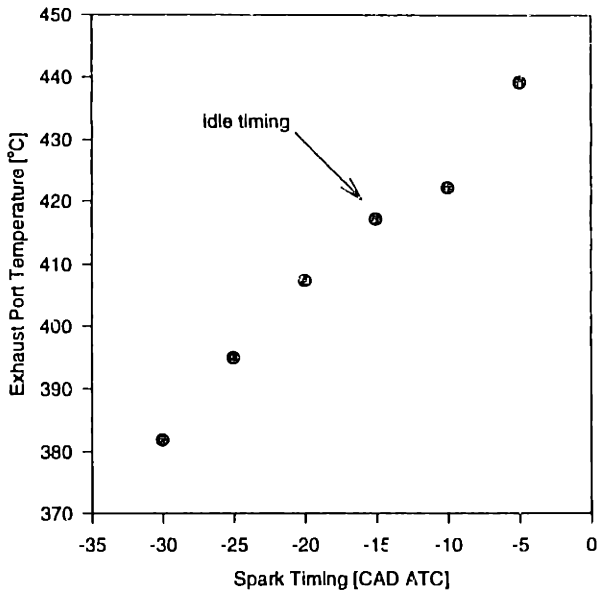


Figure 4-13. Temperature measured at the exhaust port vs. spark timing.

# 5. EXPERIMENTAL PROCEDURES

## 5.1. General Procedures

One characteristic of the cycle-to-cycle variability in an engine is that it is very operating condition sensitive. Therefore, in any effort to study cyclic variations, it is imperative that the operating condition of the engine be carefully controlled. The experiments for this study were all performed on a completely warmed up engine. The coolant temperature was kept between 80°C and 85°C, and the sump oil temperature was kept between 72°C and 77°C. With the apparatus used it was not possible to control the inlet air temperature; however, fluctuations in the ambient temperature were not significant, so inlet air temperatures stayed within a range of 25°-30°C.

As mentioned in §4.1.2, a gas flow controller was used to supply the inlet air; this enabled precise control over the air flow rate, which was kept at 0.5998 g/s. The fuel flow rate was monitored at the exhaust with a lambda sensor. For all tests, except the fuel perturbation experiments described in §5.2.4, the engine was operated at stoichiometric.

Since the air flow rate is known, the equivalence ratio is known, and the residual concentration was measured (described in §4.2.4), the average charge composition may be described, as in Table 5-1.

Table 5-1. Contents of the cylinder at idle.

| | |
|---|---|
| Air | 90 mg |
| Fuel | 6.165 mg |
| Residual | 36.29 mg |

## 5.2. Gas Perturbation Experiments

### *5.2.1. OVERVIEW*

A methodology for determining the combustion sensitivity to small changes in the charge composition is described in §3.2.2.1. A schematic of the apparatus used for the implementation of these experiments is shown in Figure 5-1. A length of 1/8" copper tubing is inserted at the left inlet port of the number 4 cylinder, approximately 2-3 centimeters from the valve. The other end of the tubing is attached to a solenoid valve (Kip, Inc. model # 141110). The perturbation gas is supplied from a regulated cylinder to a 5 gallon tank; the purpose of this tank is to keep a constant supply pressure to the solenoid valve despite the pulsing flow. A pinhole orifice is located just downstream of the solenoid valve to allow more precise control over the gas flow. Two orifices were used for the experiments in this study: 400 μm for the air and residual perturbations, and 250 μm for the fuel perturbation.

The precise amount of gas injected is controlled by the gas pressure in the 5 gallon tank and the injection pulsewidth supplied to the solenoid valve; calibrations

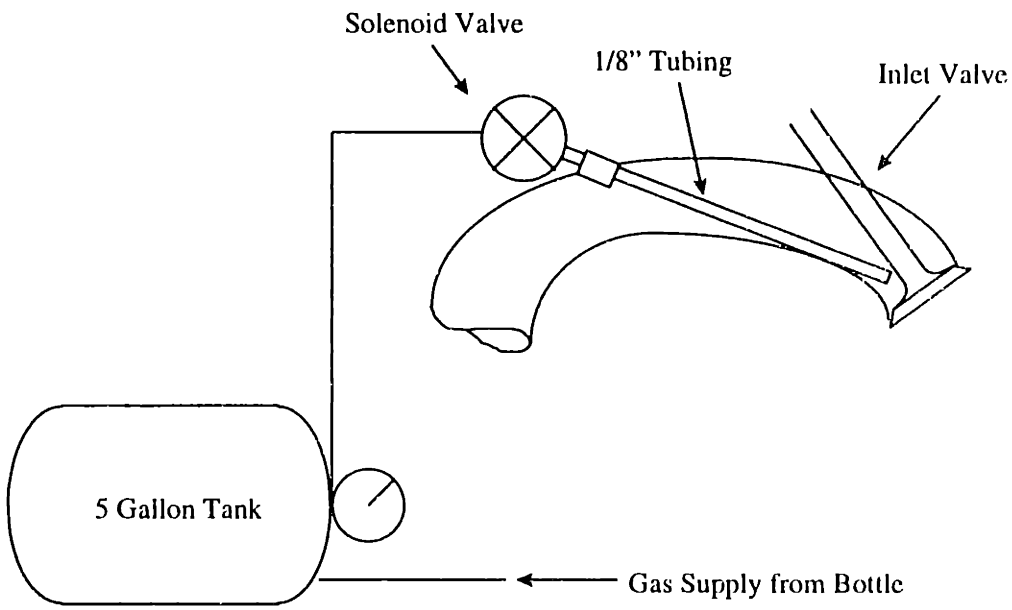


Figure 5-1. Schematic of apparatus used in gas perturbation experiments.

of the solenoid valve with both orifice sizes were performed for various supply pressures. The perturbation injection was timed to occur at 560° after BC compression—17° after EVC. Injection any earlier than this appeared to cause charge loss to the exhaust valves. Preliminary experiments showed that perturbation of every other cycle caused an obvious strong/weak cycle oscillation that confounded sensitivity results. Thus it was necessary to have a few non-perturbed cycles after the perturbed cycle to allow the combustion to "relax" back to normal; experiments indicate that three skipped cycles was a sufficient compromise between cyclic oscillations and dataset size.

As mentioned in §3.2.2.1, to ensure that the response of the combustion to the perturbations is linear, two different amounts of injection must be performed and compared. Also, it is important to note that there was no significant change in the average inlet manifold pressure as a result of the perturbations.

### *5.2.2. Residual Mass Perturbations*

Since actual residual gas, with water vapor, is difficult to handle experimentally, an artificial residual that matched the molar heat capacity of the residual gases was used in the residual mass perturbation experiments (see Appendix A for details). The largest amount of gas injected was—for the experiment with the higher injection amount—5% of the charge residual; this is less than 1.4% of the total charge mass. Experiments showed that the timing of the injection had no influence on the sensitivity results[10]; this is because the volume of injected residual is so small that it does not displace a significant amount of air during the intake process.

[10] Except for the case when injection was timed during the valve overlap period, when it appears that the momentary increase in the inlet manifold pressure caused some displacement of in-cylinder residual through the exhaust valves.

### *5.2.3. AIR MASS PERTURBATIONS*

The air perturbation experiments prove to be more difficult to implement than the residual experiments. The primary difficulty lies in the amount of gas that must be injected. Since air makes up such a large fraction of the charge, a large amount must be injected to perturb the combustion significantly[11]; thus, displacement of the normal charge intake during the inlet process is possible. Since the fresh charge that will be displaced by injection of a perturbation gas is air, a question arises as to whether the charge composition has as much "additional air" as is injected. Indeed, if air were injected to the inlet port while the inlet valve is closed, no influence on the combustion would be noted at all because the air injected would simply displace intake air. This was experimentally verified; for such experiments, there was no statistical difference between the perturbed and unperturbed cycles.

So how does one ensure that there is excess air in the cylinder? Injection of the air when the inlet valve is open causes the pressure in the inlet manifold, and thus the cylinder, to increase for a short time. This causes more air to be inducted; yet the question remains as to whether the amount injected by the solenoid valve is ingested into the cylinder. To test whether this was the case, air was injected with the solenoid every cycle, and the lambda meter was used to monitor the change in the exhaust equivalence ratio from non-perturbed operation. The change measured with the lambda meter indicated that all of the injected air was being ingested into the cylinder; that is, for a 5% perturbation, the lambda meter went from 1.00 for no perturbation to 1.05 when air was injected every cycle.

[11] This is also due to the fact that air has a weaker influence on the laminar burning velocity of a mixture than does residual. Or, put another way, the molar heat capacity of air is lower than that of residual.

### 5.2.4. *Fuel Mass Perturbation*

Since it is difficult to meter liquid fuel accurately in small amounts, the fuel perturbation experiments were performed by injecting propane at the inlet valve.[12] These experiments were performed at an air/fuel equivalence ratio of 1.05 so that the perturbation in combination with the natural cycle-to-cycle variation of the in-cylinder air/fuel ratio would not cause an equivalence ratio excursion that would bring the flame speed beyond its maximum point (which occurs at $\lambda$~0.9), which would complicate the interpretation of the sensitivities. Figure 5-2 shows the influence of relative air/fuel ratio on the IMEP at idle; the plot is quite linear for the range about 1.05, indicating that this operating condition is suitable for the fuel perturbation experiment.

It was found that, even with a small flow orifice, calibrating the solenoid valve to meter small enough amounts of propane (~ 0.2 mg) was extremely difficult, since this required operating the solenoid valve in a non-linear range.[13] It was thus necessary to find another method of measuring the requisite amount of propane to inject. For this purpose, the lambda meter was used in a manner similar to that described in §5.2.3; after the engine was running steady state at an air/fuel equivalence ratio of 1.05, propane was injected every cycle. The pulsewidth supplied to the solenoid valve was adjusted until the desired amount of perturbation was achieved;

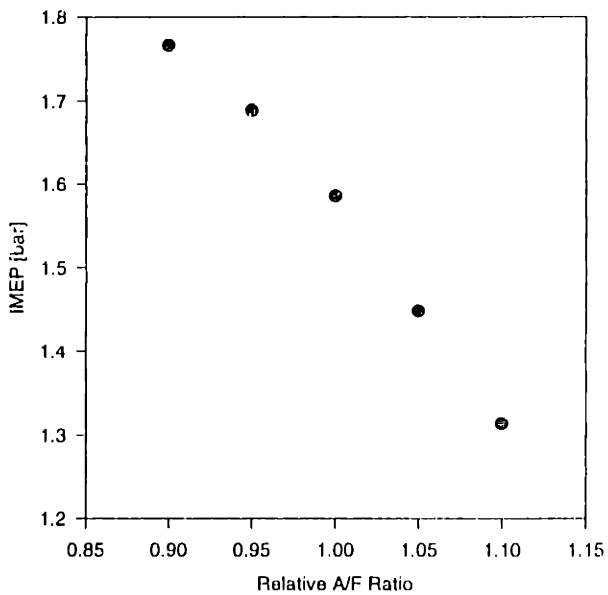


Figure 5-2. Average IMEP as a function of relative air/fuel ratio.

[12] The perturbation was performed during normal operation of the engine with port fuel gasoline injection. That is, propane was only used as the perturbation gas.

[13] This is analogous to the character of the fuel injector, which operates in a non-linear range at very low injection amounts. See Figure 1-1.

that is, for a 4% fuel perturbation, the propane injection was adjusted to give $\lambda$=1.01. Then the injection rate was set to once per four cycles, and pressure data was acquired. For the purposes of calculating the sensitivity, the fuel *energy* perturbation was the quantity considered.

## 5.3. Skip-Firing Experiments

In §3.2.2.1, the rationale for performing skip-fired experiments is presented; this section describes the experiments performed in greater detail.

The purpose of these experiments is to determine the cycle-to-cycle combustion variations that occur at idle when the influence of charge composition variations has been removed. Thus, it is important that the average combustion environment of the skip-fired experiments matches the environment of the continuously-fired experiments. Sztenderowicz [37] presents the methodology of matching skip-firing to ordinary operation in some detail; the following description relies heavily on his work.

To match the combustion environment from a continuously-fired experiment to a skip-fired experiment, there are several criteria which must be met:

1. the mean level of fluid motion must be the same between the two experiments
2. the charge laminar burning velocity (and thus, thermodynamic state) must be the same
   - charge composition must be the same
   - pressure and temperature at the time of spark must be the same

Criterion 1 may be met simply be keeping the spark timing the same; meeting criterion 2 proves to be more challenging.

Since the charge naturally contains a certain amount of residual gas—27.4% by mass, as determined in §4.2.4—it is necessary to supply some residual along with the fuel and air. Since real residual is difficult to handle, an artificial residual is used; see Appendix A for the composition of the residual. For the pressure and temperature at the time of spark to be the same, the total number of moles must be the same from one experiment to the next. Thus, the artificial residual must meet

the *molar* heating capacity of the actual residual, and the mole fraction of the artificial residual in the skip-firing case must match that of the continuously fired experiment. Table 5-1 lists the average composition of the charge; since the air flow, fuel flow, and artificial residual flow rates may all be controlled, the gas composition may be determined. However, since the skip-fired residual fraction (or the *remainder* fraction, as it is termed in [37]) is not known, the absolute amount of mass in the cylinder is not known for the skip-fired experiments. Also, the charge temperature at the inlet for the ordinary experiments is not known. These unknowns require the use of an iterative matching procedure to ensure that the skip-fired experiments adequately approximate the continuously-fired experiments.

The methodology for matching experiments used in this study is that proposed by Sztenderowicz [37]:

1. calculate the desired relative flow rates for fuel, air, and artificial residual
2. skip fire the engine at the appropriate $p_{inlet}$ and spark timing, increasing the flow rates until the IMEP matches the continuously-fired experiments
3. adjust the heating of the inlet charge until the pressure at time of spark matches the continuously-fired case.

It is necessary to iterate on steps 2 and 3 because changing the temperature of the inlet will influence the IMEP, and changing the flow rates will influence the amount of heating required to keep the inlet at a specific temperature. There is only one operating condition that will match all of the criteria.

The number of cycles that must be skipped to ensure that there is very little natural residual in the engine depends on the purge rate of the engine at the appropriate operating condition. To determine the purge rate for the Nissan at the idle condition, the engine was skip-fired with 5, 6, 7, 8, 9, and 10 skipped cycles, and pressure data were taken. The average IMEP for skipping 7 cycles was indistinguishable from the cases where more cycles were skipped between firing

cycles, so it was judged that skipping 9 cycles would be an appropriately conservative operating condition.

# 6. RESULTS AND ANALYSIS

## 6.1. Burn Parameters Used to Characterize Combustion

The experimental methodology described in Chapter 3 presupposes the knowledge of variations in certain "output" burn parameters that characterize the combustion of the idle operating condition. The fluctuations in these burn parameters are used to determine the variations in the input parameters—i.e., fuel, air, and residual mass. These burn parameters are determined on a cycle-to-cycle basis through analysis of the engine pressure data. This section discusses the choice of burn parameters for the analysis. The burn rate analysis program that was used in the analysis of the data is described in detail by Cheung [64].

An ideal set of burn parameters would characterize the combustion completely, from start to finish, as well as defining the total amount of energy released. Also, the burn parameters should be easy to determine from the cylinder pressure data, since many cycles will be taken for statistical significance. On the basis of these criteria, the following parameters were chosen for this study:

- 0-10% burn angle

- 10-50% burn angle
- 50-90% burn angle
- IMEP.

The early burn period is characterized by the 0-10% burn angle ($\theta_{0\text{-}10\%}$), also known as the flame development angle [23]; it represents the crank angle interval between spark and the time when 10% percent of the charge mass has been burned. This is often taken as a measure of the time it takes to achieve a fully developed turbulent flame in the cycle. By the time 10% of the charge mass is burned, the flame may be as large as 30% of the total combustion chamber volume.[14] Thus, the 0-2% burn angle may be preferable when the combustion period of interest is the very early flame development; however, for the sensitivity studies described in §3.2.2.2 and §5.2, it was found that the resolution of the burn rate analysis was insufficient for detecting changes in 0-2% burn angle between perturbed and non-perturbed cycles. Figure 6-1 shows a plot of the 0-10% burn angle versus the 0-2% burn angle for 500 cycles at idle. The $r^2$ value is 0.889, demonstrating a very strong correlation between the two burn parameters; this suggests that $\theta_{0\text{-}10\%}$ may be considered an adequate measure of the early stages of flame development in an engine.

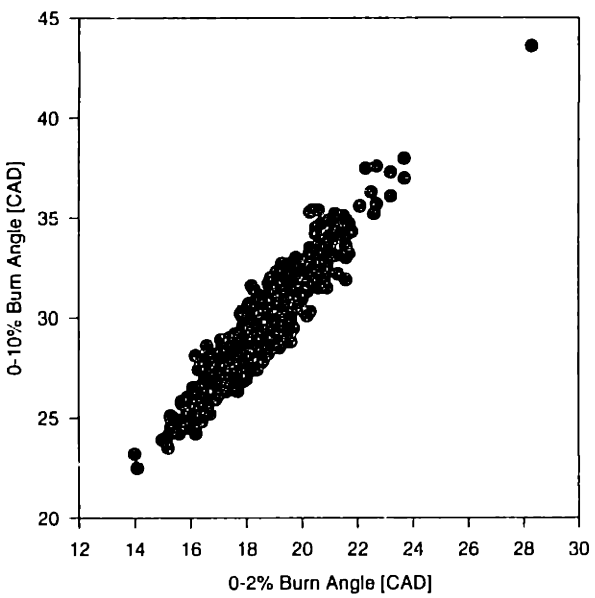


Figure 6-1. $\theta_{0\text{-}10\%}$ vs. $\theta_{0\text{-}2\%}$ for 500 cycles.

The 0-50% burn angle may be considered an approximate measure of the time it takes the flame to develop from the spark to the peak mass burning rate. The 10-50% burn angle is the earlier—and faster—part of the turbulent flame propagation, representing a significant part

[14] Assuming an unburned gas density/burned gas density ratio of about 4.

of the total rapid burning angle.[15] This portion of the combustion process is very important from a phasing standpoint; as mentioned in §4.2.2, the location of the 50% burn angle may be used as an indicator of combustion phasing with respect to optimum. Typically, the peak mass burning rate occurs within a few crank angle degrees of the 50% burn angle; thus, from this time onward combustion is slowing down. The burn speed after this point has a smaller influence on IMEP since it is so retarded with respect to the expansion stroke. Because the burned gas is substantially less dense than the unburned mixture, by the time 90% of the mass has been burned, almost the entire combustion chamber volume has been engulfed by the burned gas.

The rationale for dividing the 10-90% burn angle in half for the purposes of this analysis has to do with the phenomena that govern the flame growth in this period. During the early part of the turbulent flame propagation, flame growth is, in large part, influenced by the expansion of the burned gases behind the flame; by the time 50% of the charge mass has been burned, 80% of the combustion chamber volume has been engulfed by the flame. The later turbulent flame growth, on the other hand, is characterized by a slower flame front growth that has significant interaction with the cylinder walls. Admittedly, the division at 50% mass fraction burned is somewhat arbitrary; however, it is a convenient point to separate the early and the late turbulent flame phenomena, and it is easily defined with the analysis tools available.

[15] The 10-90% mass fraction burned angle [23].

## 6.2. Experimental Results: Charge Composition Perturbation

### *6.2.1. OVERVIEW*

The charge perturbation experiments were performed as described in §5.2. Three identical tests of 500 perturbed cycles[16] were performed for each gas at two different levels of perturbation. Table 6-1 shows the experimental matrix for the perturbation tests.

Table 6-1. Perturbation test conditions.

| Perturbation Gas | Amount injected (low/high) | % perturbation (low/high) |
|---|---|---|
| Residual | 1.10 mg/1.80 mg | 3%/5% |
| Air | 2.25 mg/3.60 mg | 2.5%/4% |
| Propane | 0.146mg/0.234mg | 2.5%/4% |

Ideally, the gas perturbation would be as small as possible, so as not to disturb the combustion too radically. However, there is the issue of detectability to consider: the perturbation must be large enough so that the analysis tools used (i.e., pressure data and burn rate analysis) can distinguish between perturbed cycles and non-perturbed cycles. The limits of detectability determine the level of gas perturbation used for the experiments.[17] Figure 6-2 shows the average pressure traces for an air perturbation experiment where the amount of excess air injected was

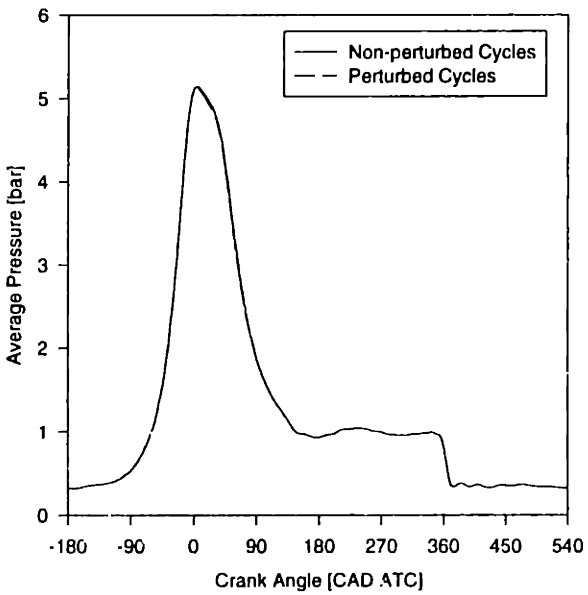


Figure 6-2. Average pressure traces for 2.5% air perturbation.

[16] The total number of cycles acquired was 2000 (4 cycles x 500).

[17] In the case of the fuel perturbation, the limiting factor was the smallest amount of propane that could be metered reliably.

2.5% of the total air mass. The non-perturbed cycles have a slightly higher pressure trace than the perturbed due to the dilution of the charge and slowing of the combustion in the latter. Also, all three non-perturbed cycles fall almost identically on top of each other so that they are indistinguishable; Table 6-2 shows the IMEP values for the cycle sequence of this air perturbation experiment. The non-perturbed cycles have average IMEP values that are less than 0.1% apart, while the perturbed cycle IMEP is approximately 1% lower than the non-perturbed cycles. This demonstrates the strength of the synchronized detection methodology—very small changes in cylinder pressure and combustion may be distinguished if a sufficient number of cycles is analyzed.

Table 6-2. Average IMEP of cycle sequence for Figure 6-2.

| Cycle | Average IMEP [bar] |
|---|---|
| Air Perturbed Cycle | 1.564 |
| Non-perturbed Cycle 1 | 1.582 |
| Non-perturbed Cycle 2 | 1.581 |
| Non-perturbed Cycle 3 | 1.583 |

### 6.2.2. *Signal to Noise Ratio*

There are two sources of noise in the perturbation experiments: the instrument error and the natural fluctuation of the physical quantities to be measured. The instrument error includes discretization and instrument noise. For the pressure measurement, the discretization error and instrument noise amounted to approximately a 1 bit fluctuation (5 mV). The signal level was ~5V; the signal to noise for a single measurement is therefore ~$10^3$. Since this noise is not synchronized with the sampling, with 500 samples, the signal to noise ratio is ~ $10^3\sqrt{500} \sim 2\times10^4$. As will be seen later, this measurement noise is small compared to the natural fluctuation of the quantity to be measured. The crank angles were measured at 1° intervals; the burn durations were determined by interpolation between crank angles, and are accurate to a fraction of a crank angle. The detectability of the perturbation depends on the size of the resulting change of

signal due to the perturbation compared to the size of the cycle-to-cycle fluctuation of the unperturbed signal. If $y_0$ and $y_1$ are the unperturbed and perturbed observations (e.g., the IMEP), the quantity we are interested in is $\Delta y$:

$$\Delta y = \bar{y}_1 - \bar{y}_0$$

The noise is

$$\left[\left(\left\langle (y_1 - \bar{y}_1)^2 \right\rangle + \left\langle (y_0 - \bar{y}_0)^2 \right\rangle\right)/(2N)\right]^{1/2}$$

Thus the signal to noise ratio is

$$\Delta y\sqrt{N}\Big/\left[\left(\left\langle (y_1 - \bar{y}_1)^2 \right\rangle + \left\langle (y_0 - \bar{y}_0)^2 \right\rangle\right)/2\right]^{1/2}$$

By using a large enough sample size (N), the signal to noise ratio could be increased substantially. Estimates of the noise uncertainty of the various quantities being measured are indicated in the results.

### *6.2.3. RESULTS*

The results for the air mass perturbations are summarized in Figures 6-3 through 6-6; each experiment was performed three times at the same condition. These graphs show the percentage change of the burn parameters specified in §6.1 as a function of the percentage perturbation. Figures 6-7 through 6-10 show the results for residual perturbations, and Figures 6-11 though 6-14 show the fuel perturbation results. The error bars represent the noise present in the signal; refer to §6.2.2 for the definition of signal to noise ratio. Note that though the signal to noise ratio is quite small for the fuel perturbation case, the repeats of the experiment fall outside of the error bar range; this is because of the difficulty in metering out the very small quantities of propane required. Refer to §5.2.4 for a brief discussion of this problem. Nevertheless, the repeatability for the fuel perturbations is quite good.

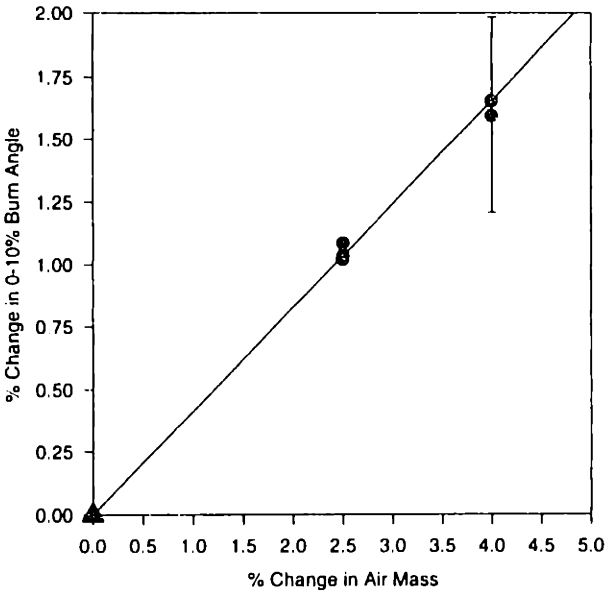


Figure 6-3. Air mass perturbation results for 0-10% burn angle.

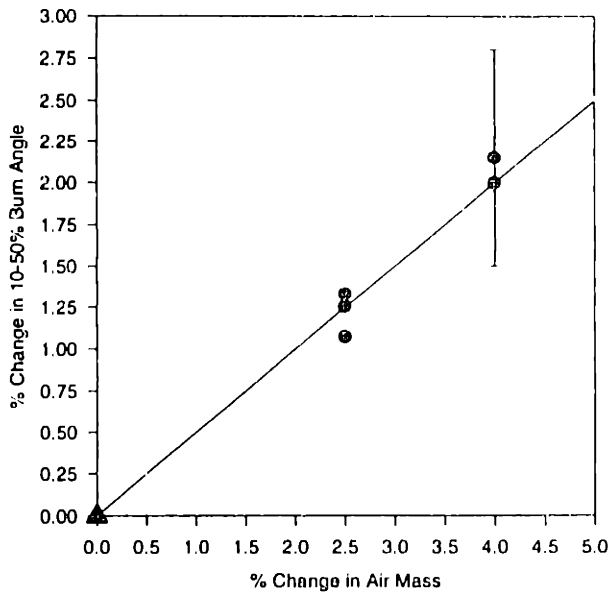


Figure 6-4. Air mass perturbation results for 10-50% burn angle.

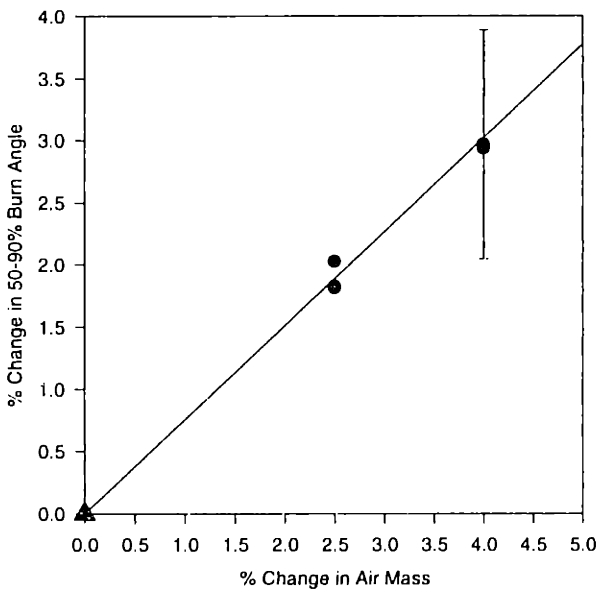


Figure 6-5. Air mass perturbation results for 50-90% burn angle.

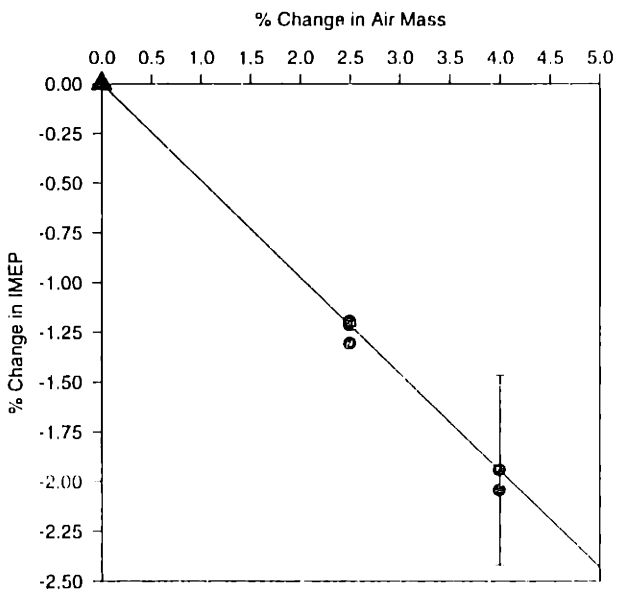


Figure 6-6. Air mass perturbation results for IMEP.

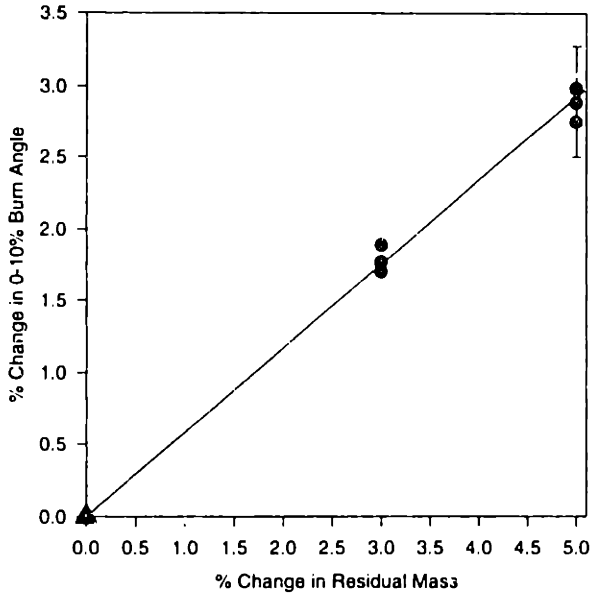


Figure 6-7. Residual mass perturbation results for 0-10% burn angle.

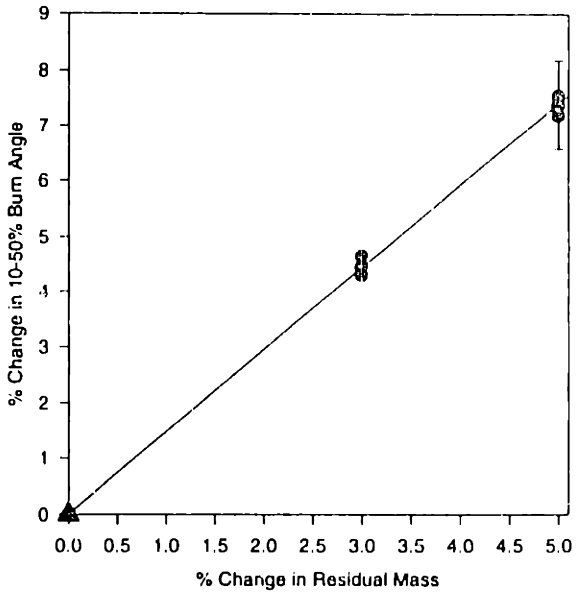


Figure 6-8. Residual mass perturbation results for 10-50% burn angle.

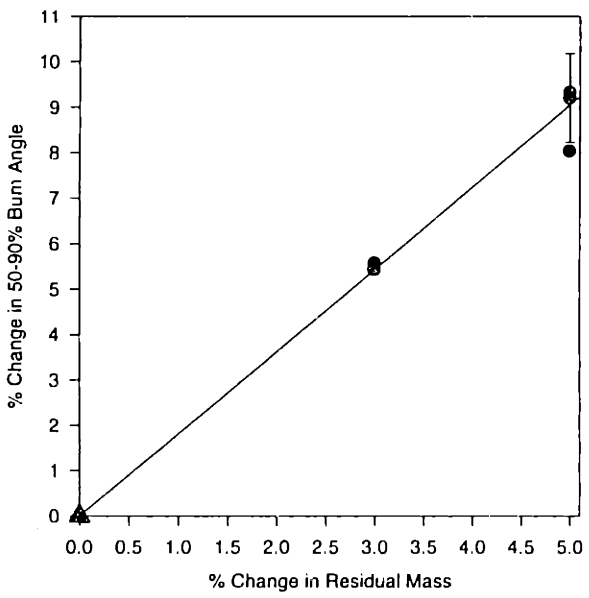


Figure 6-9. Residual mass perturbation results for 50-90% burn angle.

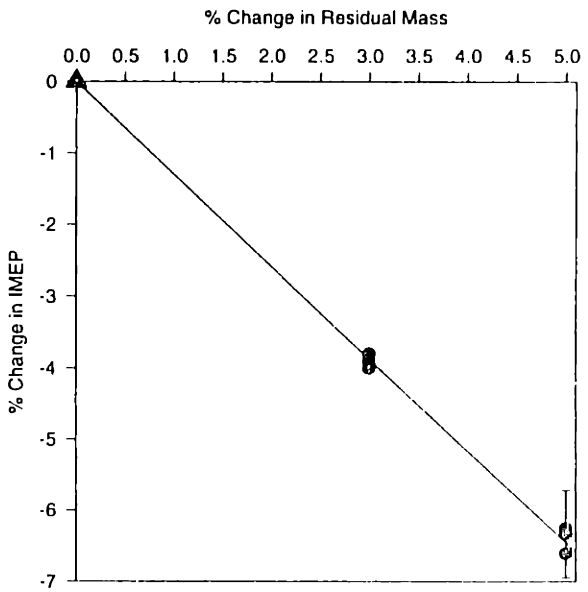


Figure 6-10. Residual mass perturbation results for IMEP.

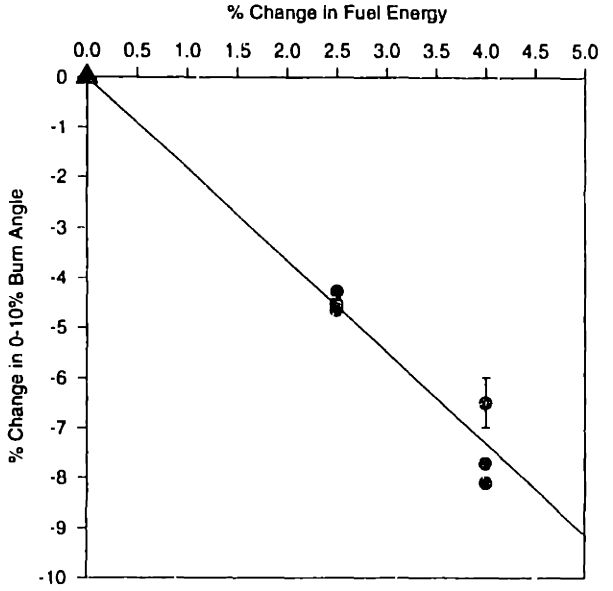


Figure 6-11. Fuel mass perturbation results for 0-10% burn angle.

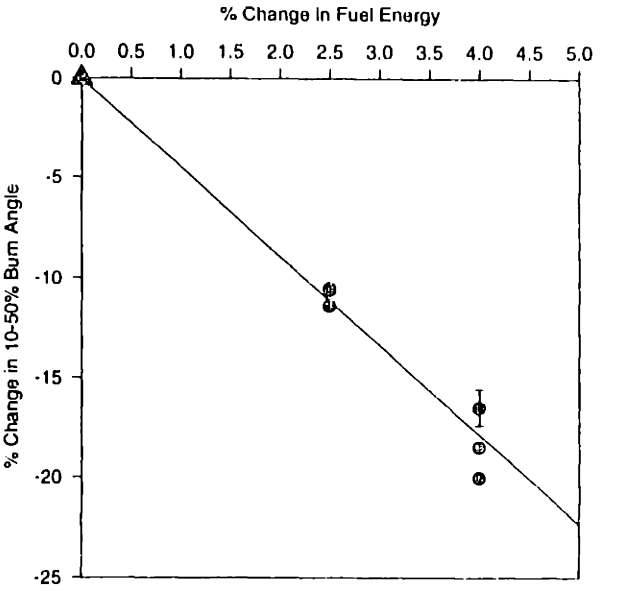


Figure 6-12. Fuel mass perturbation results for 10-50% burn angle.

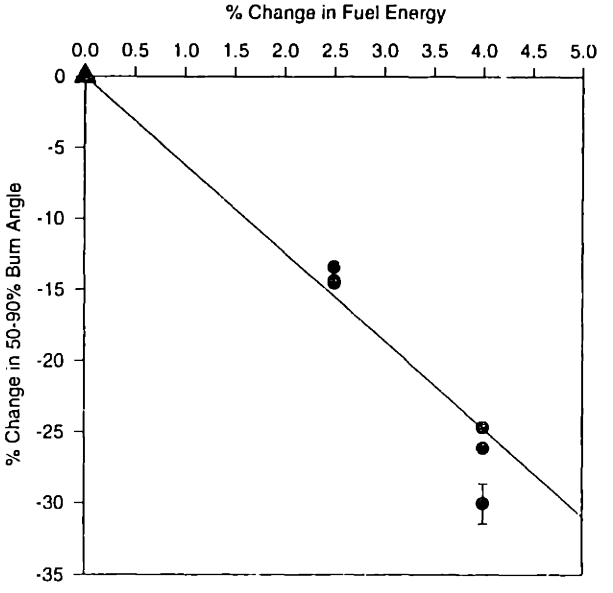


Figure 6-13. Fuel mass perturbation results for 50-90% burn angle.

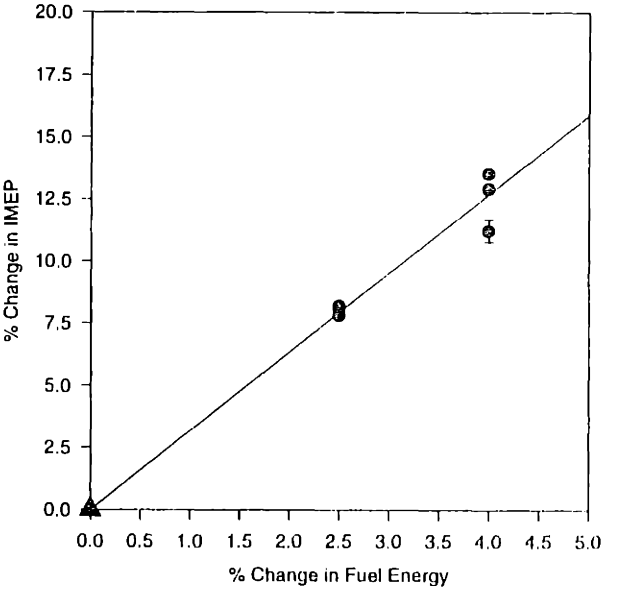


Figure 6-14. Fuel mass perturbation results for IMEP.

The results in Figures 6-3 through 6-14 show that the experiments behaved as designed: the change of the observed quantities was linearly proportional to the magnitude of the perturbation. This result confirms that the perturbation is in the linear regime. What needs to be shown *a posteriori* is that the calculated cycle-to-cycle variations in the charge component gases are within the range of these perturbation experiments; this will be done in §6.4.

The perturbation results are summarized in Figure 6-15. Comparison with the model sensitivity results (Figure 2-19) shows that the model matches the trends of the perturbations experiments quite well, though it somewhat underpredicts the fuel sensitivities; otherwise, the model and experiments are in good agreement. As expected, the residual and air perturbations cause the combustion to slow, giving a positive sensitivity for the burn angle parameters and a negative sensitivity for IMEP. That is, when the amount of residual or air in the charge is perturbed in the positive direction, the result is a longer burn time and a lower IMEP. The reverse is true for the fuel case: more fuel results in a shorter burn time and a higher IMEP.

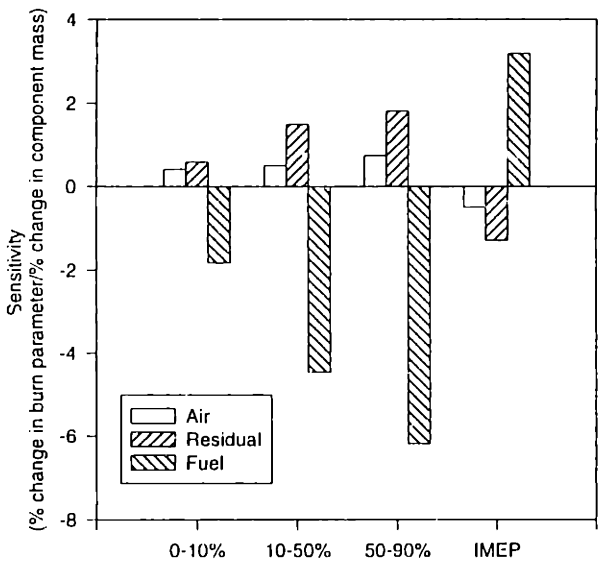


Figure 6-15. Summary of sensitivity results for air, residual, and fuel mass perturbation experiments.

There is an increase in sensitivity of the burn parameters as the cycle progresses. For example, the 50-90% burn duration is more sensitive to the perturbations than the 10-50% burn duration, which, in turn, is more sensitive than the 0-10% duration. This observation is a result of the dependence of the flame development with respect to the combustion phasing: when a flame has a fast start, the subsequent combustion occurs earlier and thus happens at a

higher pressure and temperature environment. Because of the non-linear temperature dependence of the flame speed, the burn duration for the later portion of the combustion is shortened more than the earlier part. Thus, there is an increase in the sensitivity of the "later-burn" parameters to the perturbation.

The charge perturbations influence the combustion in two different ways: they change the burn rate, and they change the total charge energy. Air and residual perturbations primarily affect the burn rate (though they do influence the charge energy somewhat), while fuel perturbations significantly influence both the burn rate and the total charge energy. The charge energy affects the engine behavior because (i) it changes the energy output per cycle, and (ii) it changes the burned gas temperature, which affects the unburned gas temperature via compression of the end gas. The unburned gas temperature then affects the laminar flame speed and thus the combustion process.

Figure 6-16 shows the calculated laminar burning velocity at the time of spark for the different perturbation experiments; the data used for this calculation are from Rhodes et al. [27] The baseline case for the fuel perturbations is different from the baseline case with the other two gases because the fuel perturbation baseline is run at a relative air/fuel ratio of 1.05, while the other two cases were run at stoichiometric; the reason for this is explained in §5.2.4. It is interesting to note that the air perturbations actually *increase* the burn rate; this is because the increase in the total charge mass reduces the residual mole fraction, and

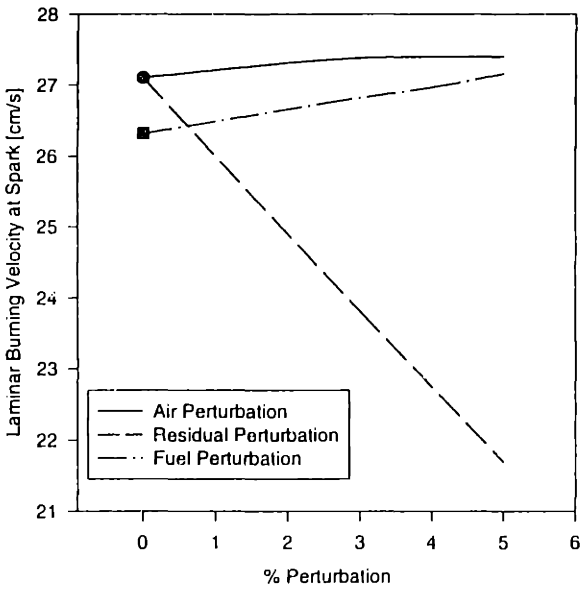


Figure 6-16. Calculated laminar burning velocity at spark for perturbation experiments.

this reduction in the residual fraction outweighs the air dilution in its influence on the laminar burning velocity. However, since the air acts as a diluent, the adiabatic burned gas temperature must be lower when there is more air. Figure 6-17 shows adiabatic burned gas temperatures for small perturbations in the component gases. The adiabatic burned gas temperature for the air perturbation is slightly higher than for the residual mass perturbation, even though a 1% perturbation in the air mass is roughly twice as much mass as a 1% residual perturbation in an absolute sense; this is due to the higher heat capacity of the $H_2O$ and $CO_2$ in the residual (or the $CO_2$ in the artificial residual). The lower burned gas temperature for the residual leads to less compression of the end gas and thus lower flame speeds due to lower unburned gas temperatures. The fuel mass perturbations have the largest influence on the adiabatic burned gas temperature—roughly twice the effect of the other two component gases.

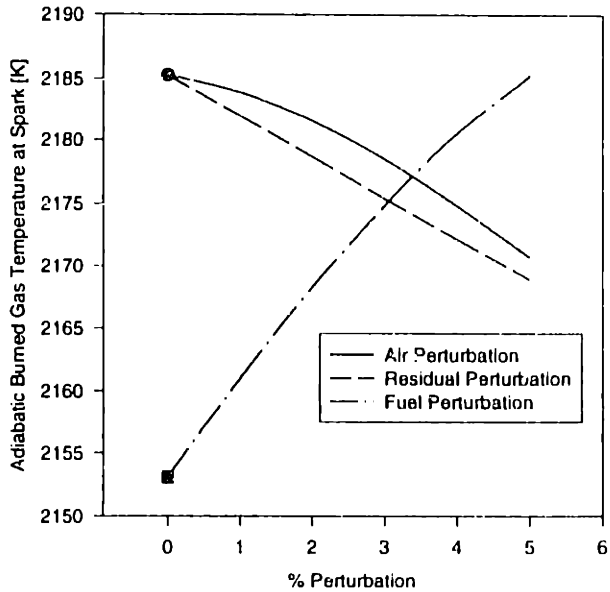


Figure 6-17. Adiabatic burned gas temperature at spark for perturbation experiments.

The difference in sensitivities of the burn parameters to the residual, air, and fuel perturbations may be explained by considering the separate influences that each component gas has on the combustion. It should be noted that the discussion applies to the same *percentage* perturbation of the three parameters; thus the actual magnitude of the air mass perturbation is substantially higher than that of the residual gas and fuel perturbations. For indolene/air combustion about the stoichiometric point, the laminar burning velocity may be expressed as the following [27]:

$$S_l = \left[b_m + b_2(\phi - 1.21)^2\right]\left(\frac{T_u}{T_0}\right)^{2.13}\left(\frac{p}{p_0}\right)^{-0.217}\left(1 - 2.06 f_d^{0.733}\right)$$

Here, $b_m$ and $b_2$ are constants, $\phi$ is the relative fuel/air equivalence ratio, $T_u$ is the unburned gas temperature, p is the cylinder pressure, $f_d$ is the mole fraction of the residual, and $T_0$ and $p_0$ are a reference temperature and pressure respectively. While $\phi$ and the residual fraction both have an influence on the burn rate, the exponent on the temperature term makes the laminar flame speed very sensitive to temperature. The laminar burning velocity has a direct influence on the turbulent burn speed (c.f. Equations 2-3 and 2-4); therefore, any changes to the laminar burning velocity will have a significant impact on the turbulent combustion rates.

When the residual gas mass increases, both the flame speed and the burned gas temperature decrease. The burned gas temperature decrease causes less rapid expansion of the flame, lowering the end gas temperature; thus the burn speed decreases and the burn duration increases. When the air mass increases, the initial flame speed increases slightly. This increase is the combined effect of a decrease in the flame speed due to a lower equivalence ratio and an increase due to the reduction of the residual gas fraction of the mixture. However, the burned gas temperature decreases because of the overall dilution, and thus the end gas temperature decreases. The latter causes a decrease in flame speed in the subsequent burning. The net effect on burn duration, however, is not as sensitive as the residual gas perturbation case which has both the flame speed factor and the end gas temperature factor. For an increase in fuel, the flame speed increases modestly due to enrichment; the enrichment is not large enough for the flame speed to overshoot its maximum value as a function of the equivalence ratio. However, the burned gas temperature, increases because of the additional energy input. The sensitivity of the burn duration to the fuel perturbation is much higher than the sensitivity to the residual perturbations. This is because, for the same percentage perturbations, the burned gas temperature response is approximately a factor of two higher for the fuel than for the residual.

The IMEP sensitivity is similar to the inverse of the burn duration, though it is a result of both the combustion phasing and the total energy content of the charge. That is to say, any decrease in burn duration will result in an increase in IMEP, and an increase in total charge energy—most significant in the fuel perturbation case—will also cause an increase in the IMEP.

## 6.3. Skip Fired Experiments

### *6.3.1. Matching the Continuously Fired Case*

As described in §5.3, the operating condition for the skip-fired experiments must be matched to that of the ordinary continuously-fired experiments. Figure 6-18 shows a comparison of the mean results for skip firing and continuously-firing cases. Each test was performed three times; there are 2000 cycles taken for the continuous firing case and 500 cycles taken for the skip-fired experiments. Repeatability proves to be good for both sets of experiments. Also, there are no significant differences between burn parameters in the continuous-firing and skip-firing experiments, indicating that the matching described in §5.3 was successful.

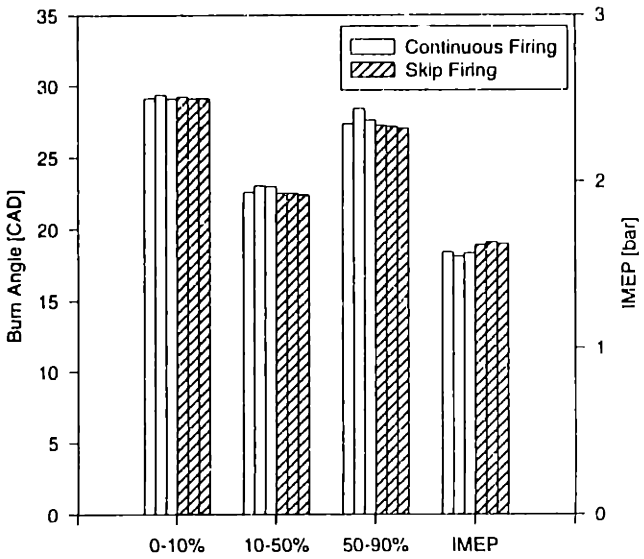


Figure 6-18. Comparison of mean results for continuous firing and skip firing operation.

### *6.3.2. Comparison of Variations*

Figure 6-19 shows a comparison of the COVs for the continuously-fired and the skip-firing cases; again, repeatability is good from test to test. The COVs of the skip-fired experiments are noticeably lower than the continuous-fired experiments by design. The differences between the skip-fired and the continuously-fired variability may be attributed to variations of the charge air, fuel, and residual masses.

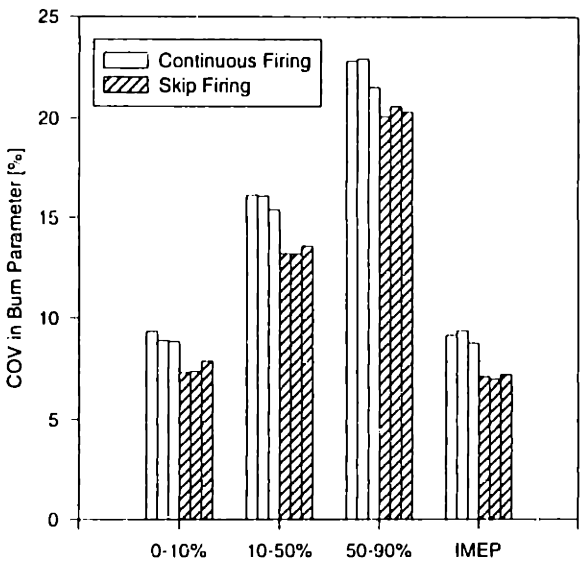


Figure 6-19. Comparison of continuously fired and skip fired variation results.

Figure 6-20 shows the percent reduction in the COVs achieved in the skip-fired experiments. Note that there is approximately a 20% reduction in the IMEP variations; Sztenderowicz [37] found a 50% reduction in IMEP variations through skip-fired experiments at a low speed, low load case. The difference may attributed to abnormal combustion cycles in his data; there were no misfires in either set of experiments presented here, and there were fewer than 0.1% partial burns in the continuously-fired case.

Figure 6-20 shows that the largest reduction in the variability occurs in the early portion of the combustion. This result is consistent with the influence that mixture composition variations have on the combustion rates. Early in the combustion, the laminar burning velocity—and thus, the mixture composition—dominates the flame speed. Therefore, eliminating the cycle-to-cycle variability in the composition should reduce the variability the most early on in the combustion event. Later in the cycle, turbulence has a dominant role in the flame speed, and the influence of mixture composition on cycle-to-cycle variations becomes less important. Also,

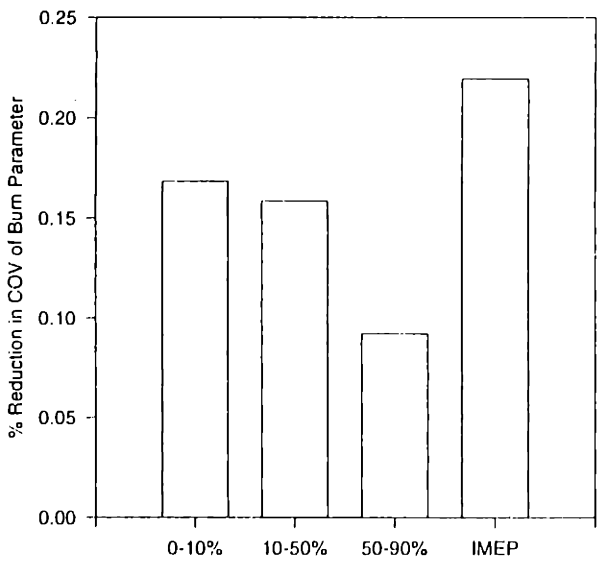


Figure 6-20. Percent reduction in burn parameter COV from continuous firing to skip firing.

variations in the contact area of the enflamed volume with the combustion chamber geometry will have the largest influence late in the cycle, since it is only then that the flame will be large enough to interact significantly with the combustion chamber walls.

It should be noted that the difference in variability between the skip-fired experiments and the continuous-fired experiments does not perfectly isolate the charge composition variations. Mixture inhomogeneities are also eliminated with skip-firing, and it is impossible to separate the influence of this effect from the charge composition variation effect. However, since mixture inhomogeneities should have a lesser effect as the flame grows because the local fluctuations become "averaged out" over the larger flame area [33], and since the earliest burn parameter that is considered in this study is the 0-10% burn angle (at which point the enflamed volume occupies almost one third of the combustion chamber volume), for the purpose of the analysis that follows it is assumed that the overall composition variations are more important than mixture inhomogeneities.

Note also that the skip-firing experiments completely eliminate the *relative* composition variations; there is no guarantee that the total charge mass will not vary from one skip-fired cycle to the next. However, the gas exchange process is much more repeatable for the skip-fired operation (which is essentially the same as motored operation) than it is for continuous-firing, so the overall mass fluctuations should be of significantly smaller magnitude.

## 6.4. Analysis of Charge Composition Variations

### *6.4.1. RESULT*

Table 6-3 shows the results of the calculation outlined in §3.2. The leftmost column is the column vector $(\eta_j^2 - \eta_{j,0}^2)$, which is the difference between the $COV^2$ of the burn parameters ($\theta_{0\text{-}10\%}$, $\theta_{10\text{-}50\%}$, $\theta_{50\text{-}90\%}$, and IMEP) for the continuously-fired experiments (C.F.) and the skip-fired experiments (S.F.); these are the measured "outputs." Next in the table is the sensitivity matrix $\mathbf{D}_{j,i}$. The three columns are for a perturbation of the air mass, residual mass, and fuel mass respectively; each row is for a burn parameter. That is, column 1 row 1 represents $\partial \ln \theta_{0-10\%} / \partial \ln m_{air}$, column 2 row 1 is $\partial \ln \theta_{0-10\%} / \partial \ln m_{residual}$, and so on.

Finally, the rightmost portion of Table 6-3 shows $\zeta_i^2$, the calculated results for the "input" variations in the component gas masses. These numbers—5.5% for air, 4.4% for residual, and 0.64% for fuel—represent the percent variations in th charge composition on a cycle-to-cycle basis. Thus, the mass of air in the cylinder varies the most cycle-to-cycle, and the mass of fuel varies the least. Comparison of these results with the experimental conditions for the perturbation experiments shows that the percent variations in the gases are within the linear range of sensitivities.

By multiplying the input variation vector, $\zeta_i^2$, with the sensitivity matrix $\mathbf{D}_{j,i}$, the contribution of each component mass variation to the overall variations in the

Table 6-3. Results of analysis of charge composition variations.

| $\eta_j^2-\eta_{j,0}^2$ | | $D_{j,i}$ | | | $\zeta_i^2$ | | $\zeta_i$ |
|---|---|---|---|---|---|---|---|
| $\{COV^2_{C.F.}-COV^2_{S.F.}\}$ | | $m_{air}$ | $m_{residual}$ | $m_{fuel}$ | $COV^2$ | | COV |
| $0.0902^2-0.0750^2$ | $\theta_{0\text{-}10\%}$ | $0.414^2$ | $0.586^2$ | $1.827^2$ | $3.03\times10^{-3}$ | $m_{air}$ | 5.5% |
| $0.158^2-0.133^2$ | $\theta_{10\text{-}50\%}$ | $0.499^2$ | $1.484^2$ | $4.463^2$ | $1.90\times10^{-3}$ | $m_{residual}$ | 4.4% |
| $0.224^2-0.203^2$ | $\theta_{50\text{-}90\%}$ | $0.735^2$ | $1.810^2$ | $6.190^2$ | $4.11\times10^{-5}$ | $m_{fuel}$ | 0.64% |
| $0.0908^2-0.0709^2$ | IMEP | $0.486^2$ | $1.290^2$ | $3.182^2$ | | | |

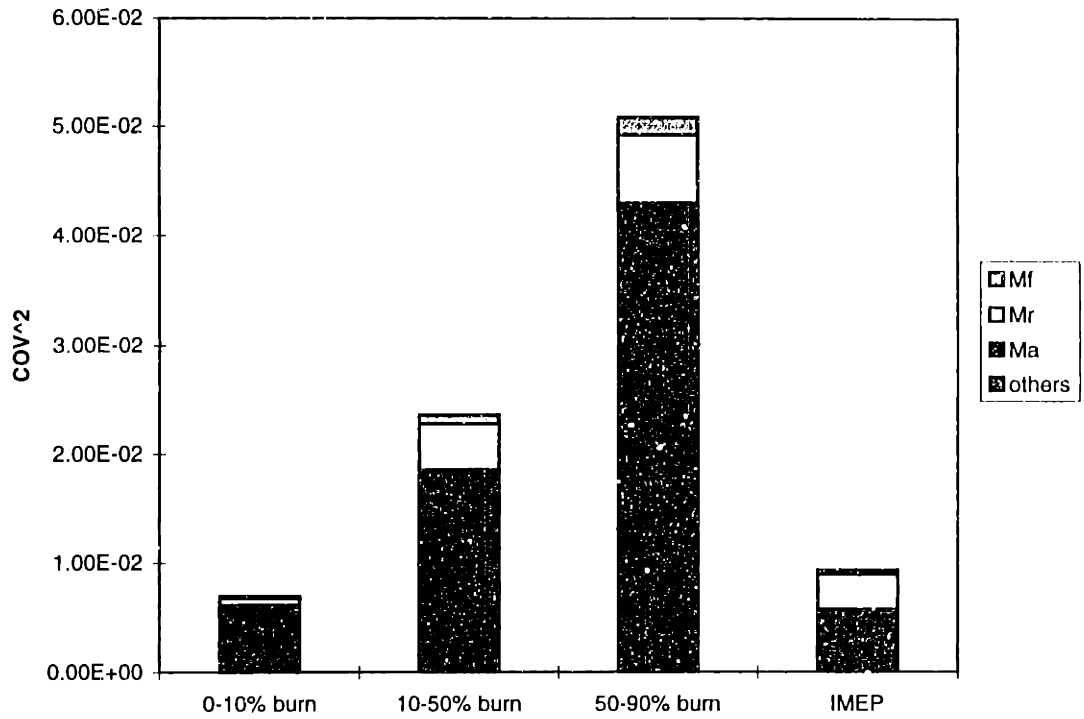


Figure 6-21. Contribution of variations in each component gas to the overall $COV^2$ of the burn parameters.

burn parameters may be determined. Figure 6-21 shows the contributions of the variations in each component gas to the $COV^2$ of the burn parameters. The contribution due to the "others"—which may be mainly attributed to fluid motion, which cannot be tested in the perturbation experiment—is more than half of the total variation. The contributions due to the charge component variations, however, are also significant. Of the component gases, the residual gas variations have the largest influence on all of the combustion parameter fluctuations; in particular variations in residual contribute to 1/3 of the total $COV^2$ of the IMEP. The contributions of the air and the fuel variations, on the other hand, are much smaller: 7.5% and 4.6% of the $COV^2_{IMEP}$ respectively.

Figure 6-22 shows the same result as Figure 6-21, with the results recast in terms of the size of the individual COV contributions. Each component bar in this

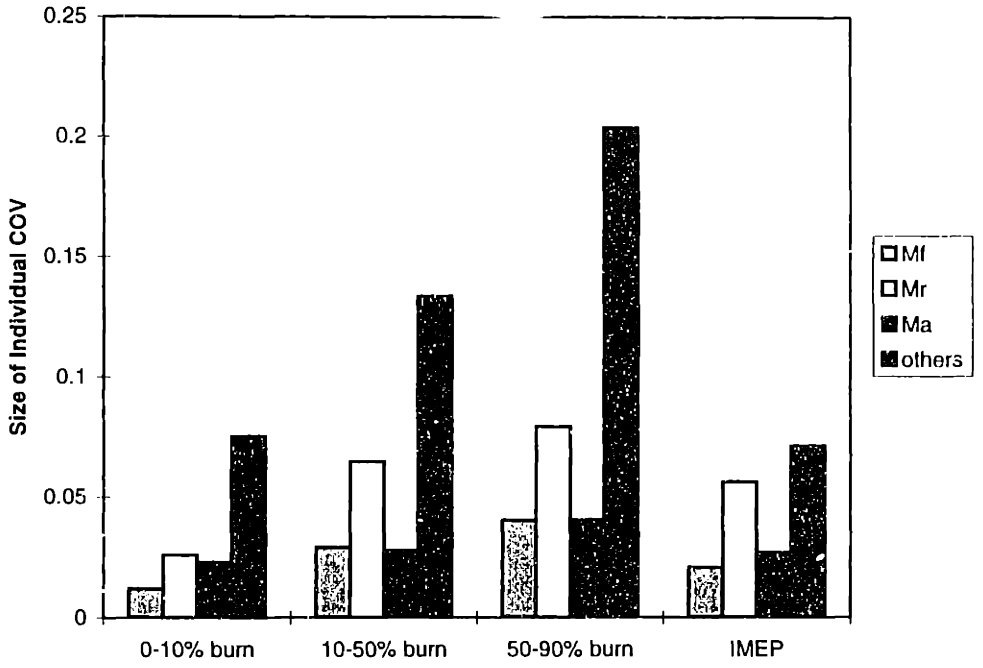


Figure 6-22. Individual contribution of variations in each component gas to the COV of the burn parameters.

graph represents the size of the COV of the output parameters if all of the other influences were eliminated. Thus, the "others" bar is the COV determined from the skip-fired experiments, since composition variations were eliminated in that case. Again, of the charge component variations, the residual mass variations represent the most significant contributor, with the air and fuel contributions being of the same order.

### *6.4.2. Uncertainty Analysis of the Sensitivity Matrix*

In §6.2.2, the signal to noise ratio of the gas perturbation experiments was discussed. The noise in the data create an uncertainty in the calculated sensitivities; Appendix B describes how these uncertainties in the sensitivities were determined. The uncertainties in the various sensitivities is shown in Table 6-4. As this table shows, there are some rather large uncertainties in the air sensitivity calculation. This is because the burn parameters are much less sensitive to the air

Table 6-4. Uncertainties in burn parameter sensitivities.

| Burn Parameter | $m_{air}$ | $m_{residual}$ | $m_{fuel}$ |
|---|---|---|---|
| 0-10% Burn Angle | 13% | 6.6% | 3.4% |
| 10-50% Burn Angle | 20% | 6.1% | 2.6% |
| 50-90% Burn Angle | 16% | 5.5% | 2.9% |
| IMEP | 14% | 3.8% | 2.9% |

perturbation, so that the signal of the perturbation experiments was substantially smaller while the noise remained the same. These uncertainties will result in uncertainties in the component gas variation results. The uncertainties calculated in the individual fluctuations of the component gases are shown in Table 6-5. The largest uncertainty, by far, is in the air mass calculation, at 100%. However, since the sensitivity of the combustion to changes in the air mass is the lowest, the net effect of these uncertainties on the results presented in Figures 6-21 and 6-22 is that it does not change the ranking of the sources. That is to say, despite the large uncertainties in the calculation, the fluctuations in the residual mass are the most significant contributor to cycle-to-cycle variability.

Table 6-5. Uncertainty in the calculated COV of the charge components.

| Component | Uncertainty |
|---|---|
| $m_{air}$ | 100% |
| $m_{residual}$ | 18% |
| $m_{fuel}$ | 33% |

### *6.4.3. Other Sources of Uncertainty in the Methodology*

One of the assumptions made in the description of the experimental methodology (Chapter 3) was that fluctuations in the input variations were uncorrelated (or that the cross-correlation terms are small compared to the auto-correlation terms). This assumption was necessary to eliminate the cross-correlation terms and limit the number of unknowns. However, the air mass and

residual mass fluctuations are not completely uncorrelated, since the amount of residual may affect the air mass during the charging process. The residual mass may increase as a result of several phenomena, each possibly having a different influence on the air mass inducted. If the overlap period increases as a result of the hydraulic lifter dynamics (c.f. §1.3.1), there will be more residual because of increased backflow, and air will be displaced by the residual; thus there may be a negative correlation between $m_a$ and $m_r$. On the other hand, the residual mass may increase because of a decrease in the exhaust temperature of the previous cycle due to combustion speed variations (i.e., a cycle that is faster with respect to average). In this case one may argue that the air mass will actually increase as a result because there will be less heat transfer from the residual to the air, and thus the air density will be higher; thus there may be a positive correlation between $m_a$ and $m_r$. The magnitude of the cross-correlation between the cycle-to-cycle fluctuations in air and residual is therefore difficult to estimate; hence its exact influence on the analysis presented above could not be assessed.

# 7. SUMMARY AND CONCLUSIONS

The objective of this work was to identify and quantify the most significant sources of cycle-to-cycle combustion variability in a spark-ignition engine at idle. However, since the causes of cycle-to-cycle combustion variations are many, the focus of this study was placed on several key phenomena:

1. cycle-to-cycle variations in turbulence
2. cycle-to-cycle variations in bulk flow
3. cycle-to-cycle variations in charge composition.

These factors were chosen on the basis of a literature survey and the specific characteristics of the idle operating condition.

A modeling study using an adapted quasi-dimensional cycle simulation indicated that the combustion was most sensitive (in order) to changes in

1. fuel mass
2. residual mass

3. charge turbulence

4. air mass.

The modeling study also indicated that variations in bulk gas flow velocities, which influence the speed and direction in which the flame is convected, did influence combustion variability, though to a much lesser extent than did the other four parameters. However, explicit conclusions were difficult to make because the variations in the in-cylinder environment were not known.

To determine the charge composition variations, a methodology was developed whereby the input variations in air mass, fuel mass, and residual mass could be identified through analysis of the variations in the output burn parameters (i.e., the 0-10% burn angle, 10-50% burn angle, 50-90% burn angle, and IMEP). To determine the sensitivity of the output burn parameters to small changes in composition, a set of novel charge composition perturbation experiments were performed. On a cycle-to-cycle basis, a small amount of one of the component gases was added to the normal charge. Analysis of the perturbed and the unperturbed cycles showed a detectable change in the combustion parameters. Fuel perturbations had the largest effect, followed by residual perturbations and air perturbations. These results were consistent with the modeling study and with calculations of the perturbed changes in flame speed and burned gas temperature.

Skip-firing engine experiments, in which all mixture composition variations were eliminated, indicated that charge composition variations do contribute significantly to cycle-to-cycle combustion variations. The burn duration variations were reduced by 10-15% and the IMEP variations were reduced by over 20%. Furthermore, the variations in the burn parameters at the early phases of combustion showed a larger reduction than those at the later phases as a result of skip-firing. This is consistent with the influence of charge composition on the combustion; charge composition has a relatively

larger effect on the early phases of combustion, and gas flow variations have more influence on the later portions. Thus, elimination of charge composition variations should have the most influence early in the cycle.

Least squares analysis of the set of linear sensitivity equations gave a result for the variations in the component gases: air 5.5%, residual 4.4%, and fuel 0.6%; these levels of variation are within the linear range used in the perturbation experiments. However, the sensitivity of the combustion to air mass variations is smallest of the three components; thus, among the charge components, residual gas mass fluctuations were found to be the most significant contributor to the cycle-to-cycle combustion variations. The contribution of air and fuel fluctuations were of the same order. Analysis of the signal to noise ratio of the perturbation experiments indicated that there was quite a large uncertainty in the component mass variations calculated; however, despite the uncertainties, the residual mass variation remains the most important factor in the combustion variations. It should be stressed that the application of the results of this study are limited to the experimental condition and the apparatus used. The effect of charge composition variations on combustion variability will be influenced by the particular engine geometry and charging characteristics, as well as the operating condition.

The results of this study suggest that the most profitable avenue of investigation for reducing cycle-to-cycle combustion variations would be to determine and control the sources of residual mass variations; it is estimated that if the residual mass fluctuations were eliminated, the COV of the IMEP could be reduced by 20% (i.e., two percentage points at a COV of 10%). Absolute elimination of variations in residual is impossible; however significant reductions in the variability might be realized through improved design. In particular, experiments to determine whether valve overlap variations due to hydraulic valve lifters are a significant contributor to

variability in the residual mass would indicate whether combustion variations may be reduced with a better valve/cam/lifter design.

# 8. APPENDICES

## 8.1. Appendix A: Composition of Artificial Residual

Since the presence of water vapor in actual residual gas makes it difficult to handle in the context of an engine experiment, it was necessary to use a synthetic residual for the residual gas perturbation and the skip-firing experiments. Residual gas-at stoichiometric operation-is composed primarily of $N_2$, $CO_2$ and $H_2O$. The synthetic residual consisted of $N_2$ and $CO_2$; since $H_2O$ has a higher heat capacity than $N_2$, additional $CO_2$ must be added to match the molar heating capacity.

Sztenderowicz [37] developed the following equation for $CO_2$ concentration in the artificial residual:

$$y_{CO_2} = y'_{CO_2} + \chi y'_{H_2O}$$

Here $y_{CO2}$ is the $CO_2$ mole fraction in the synthetic residual, $y'_{CO2}$ and $y'_{H2O}$ are the $CO_2$ and $H_2O$ concentrations in the actual residual, and $\chi$ is given by the following equation:

$$\chi = \left(\tilde{c}_{p,H_2O} - \tilde{c}_{p,N_2}\right) \Big/ \left(\tilde{c}_{p,CO_2} - \tilde{c}_{p,N_2}\right)$$

where $\tilde{c}_{p,i}$ is the molar heating capacity of component i.. At the idle condition, the temperature at spark is on the order of 750K, and at peak pressure the unburned gas temperature is closer to 800K. Data from the *Jannaf Thermochemical Tables* [65] were used to calculate $\chi$. For this temperature range, $\chi$ does not vary much; a value of 0.37 was chosen as an appropriate average over the range of interest. For indolene/air combustion, this results in a residual gas composition of 18% $CO_2$ and 82% $N_2$ by volume.

## 8.2. Appendix B: Estimate of the error in slope for a forced fit of a line through the origin

Consider a set of data points $(x_i, y_i)$ with error bars $\sigma_i$, that fit a line y=bx. The error may be represented as

$$L^2 = \sum_i \frac{(bx_i - y_i)^2}{\sigma_i^2}$$

To minimize this error, set $\frac{\partial L^2}{\partial b} = 0$:

$$\sum_i \frac{2(bx_i - y_i)}{\sigma_i^2}(x_i) = 0$$

Solving for b,

$$b = \frac{\sum_i (x_i y_i / \sigma_i^2)}{\sum_i \frac{x_i^2}{\sigma_i^2}}.$$

The uncertainty in b is

$$\sigma_b^2 = \sum_i \left(\frac{\partial b}{\partial y_i}\right)^2 \sigma_i^2,$$

and

$$\frac{\partial b}{\partial y_i} = \frac{(x_i/\sigma_i^2)}{\sum_i \frac{x_i^2}{\sigma_i^2}}.$$

Combining the above and taking the square root gives the uncertainty for b:

$$\sigma_b = \sqrt{1 \Big/ \left(\sum_i \left(\frac{x_i^2}{\sigma_i^2}\right)\right)} \qquad (*)$$

This is the equation that was used in §6.4.2 to calculate the uncertainty in the gas perturbation sensitivities.

# 9. REFERENCES


1. Young, M.B., "Cyclic Dispersion in the Homogeneous-Charge Spark-Ignition Engine—A Literature Survey," SAE Paper 810020, 1981.

2. Soltau, J.P., "Cylinder Pressure Variations in Petrol Engines," *Proceedings of the Institution of Mechanical Engineers*, Vol. **2**, 1960-1961.

3. Ozdor, N., Dulger, M., and Sher, E., "Cyclic Variability in Spark Ignition Engines—A Literature Survey," *SAE Transactions*, Vol. **103**, pp. 1514-1552, 1994.

4. Bates, S.C., "Flame Imaging Studies of Cycle-by-Cycle Combustion Variation in a SI Four-Stroke Engine," SAE Paper 892086, 1989.

5. Herweg, R., Begleris, Ph., Zettlitz, A., and Ziegler, G.F.W., "Flow Field Effects on Flame Kernel Formation in a Spark-Ignition Engine," SAE Paper 881639, 1988.

6. Hacohen, J., Belmont, M.R., Yossefi, D., Thomas, J.C., and Thurley, R., "The Effect of Flame Kernel Surface Stretch on Cyclic Variability in an S.I. Engine," SAE Paper 932717, 1993.

7. Johansson, B., "Influence of the Velocity Near the Spark Plug on Early Flame Development," SAE Paper 930481, 1993.

8. Le Coz, J.F., Deschamps, B., and Baritaud, T.A., CEC/NUTEK/JRC Homogeneous Combustion Project Meeting, Rueil-Malmaison, January 1994.

9. Keck, J.C., Heywood, J.B., and Noske, G., "Early Flame Development and Burning Rates in Spark Ignition Engines and Their Cyclic Variability," SAE Paper 870164, 1987.

10. Bradley, D., Hynes, J., Lawes, M., and Sheppard, C.G.W., "Limitations to turbulence-enhanced burning rates in lean burn engines," *Proceedings of the Institution of Mechanical Engineers*, Vol. **3**, 1988.

11. Blint, R.J., "Stretch in Premixed Laminar Flames Under IC Engine Conditions," *Combustion Science and Technology*, Vol. **75**, pp. 115-127, 1991.

12. Abdel-Gayed, R.G., Bradley, D., Lawes, M., and Lung, F.K-K., "Premixed Turbulent Burning in Explosions," *Twenty-First Symposium (International) on Combustion, The Combustion Institute*, pp. 497-504, 1986.

13. Kalghatgi, G.T., "Early Flame Development in a Spark-Ignition Engine," *Combustion and Flame*, Vol. **60**, pp. 299-308, 1985.

14. Gatowski, J.A., Heywood, J.B., and DeLaplace, C., "Flame Photographs in a Spark-Ignition Engine," *Combustion and Flame*, Vol. **56**, pp. 71-81, 1984.

15. Ho, C.M., and Santavicca, D.A., "Turbulence Effects on Early Flame Kernel Growth," SAE Paper 872100, 1987.

16. Bianco, Y., Cheng, W.K., and Heywood, J.B., "The Effects of Initial Flame Kernel Conditions on Flame Development in SI Engines," SAE Paper 912402, 1991.

17. Baritaud, T.A., "High Speed Schlieren Visualization of Flame Initiation in a Lean Operating S.I. Engine," SAE Paper 872152, 1987.

18. Ting, D.S-K., Checkel, M.D., Johansson, B., "The Importance of High-Frequency, Small-Eddy Turbulence in Spark Ignited, Premixed Engine Combustion," SAE Paper 952049, 1995.

19. Hill, P.G., "Cyclic Variations and Turbulence Structure in Spark-Ignition Engines," *Combustion and Flame*, Vol. **72**, pp. 73-89, 1988.

20. Hill, P.G., "The Relationship Between Cyclic Variations in Spark-Ignition Engines and the Small Structure of Turbulence," *Combustion and Flame*, Vol. **78**, pp. 237-247, 1989.

21. Blizard, N.C., and Keck, J.C., "Experimental and Theoretical Investigation of Turbulent Burning Models for Internal Combustion Engines," SAE Paper 740191, *SAE Transactions*, Vol. **83**, 1974.

22. Keck, J.C., "Turbulent Flame Structure and Speed in Spark-Ignition Engines," *Nineteenth Symposium (International) on Combustion, The Combustion Institute*, pp. 1451-1466, 1982.

23. Heywood, J.B., Internal Combustion Engine Fundamentals, McGraw-Hill, 1988.

24. Witze, P.O., Martin, J.K., and Borgnakke, C., "Conditionally-Sampled Velocity and Turbulence Measurements in a Spark Ignition Engine," *Combustion Science and Technology*, Vol. **36**, pp. 301-317, 1984.

25. Metghalchi, M., and Keck, J.C., "Laminar Burning Velocity of Propane-Air Mixtures at High Temperature and Pressure," *Combustion and Flame*, Vol. **38**, pp. 143-154, 1980.

26. Metghalchi, M., and Keck, J.C., "Burning Velocity of Mixtures of Air with Methanol, Isooctane, and Indolene at High Pressure and Temperature," *Combustion and Flame*, Vol. **48**, pp. 191-210, 1982.

27. Rhodes, D.B., and Keck, J.C., "Laminar Burning Speed Measurements of Indolene-Air-Diluent Mixtures at High Pressures and Temperatures," ," SAE Paper 850047, *SAE Transactions*, Vol. **95**, 1985.

28. Gülder, Ö.L., "Laminar Burning Velocities of Methanol, Isooctane, and Isooctane/Methanol Blends," *Combustion Science and Technology*, Vol. **33**, pp. 179-192, 1983.

29. Bradley, D, Habik, S.E-D., and El-Sherif, S.A., "A Generalization of Laminar Burning Velocities and Volumetric Heat Release Rates," *Combustion and Flame*, Vol. **87**, pp. 336-346, 1991.

30. Lawrenz, W., Köhler, J., Meier, F., Stolz, W., Wirth, R., Bloss, W.H., Maly, R.R., Wagner, E., and Zahn, M., "Quantitative 2D LIF Measurements of Air/Fuel Rations During the Intake Stroke in a Transparent SI Engine," SAE Paper 922320, 1992.

31. Shimizu, R., Matumoto, S., Furuno, S., Murayama, M., and Kojima, S., "Measurement ofAir-Fuel Mixture Distribution in a Gasoline Engine Using LIEF Technique," SAE Paper 922356, 1992.

32. Hiltner, J., and Samimy, M., "A Study of In-Cylinder Mixing in a Natural Gas Powered Engine by Planar Laser-Induced Fluorescence," SAE Paper 961102, 1992.

33. Berckmüller, M., Tait, N.P., and Greenhalgh, D.A., "The Influence of Local Fuel Concentration on Cyclic Variability of a Lean Burn Stratified-Charge Engine," SAE Paper 970826, 1997.

34. Hamai, K., Kawajiri, H., Ishikuza, T., and Nakai, M., "Combustion Fluctuation Mechanism Involving Cycle-to-Cycle Spark Ignition Variation Due to Flow Motion in S.I. Engines," *Twenty-first Symposium (International) on Combustion, The Combustion Institute*, pp. 505-512, 1986.

35. Baritaud, T.A., "Optical and Numerical Diagnostics for SI Engine Combustion Studies," The Third International Symposium on Diagnostics and Modeling of Combustion in Internal Combustion Engines, July 11-14, Yokohama, Japan, COMODIA 94, pp. 43-51, 1994.

36. Lee, K-H., and Foster, D.E., "Cycle-by-Cycle Variations in Combustion and Mixture Concentration in the Vicinity of the Spark Plug Gap," SAE Paper 950814, 1995.

37. Sztenderowicz, M.L., "Mixture Nonuniformity and Combustion Variability in Spark Ignition Engines," Ph.D. Thesis, Mech. Eng. Dept. MIT, 1989.

38. Grünefeld, G., Beushausen, V., Andresen, P., and Hentschel, W., "A Major Origin of Cyclic Energy Conversion Variations in SI Engines: Cycle-by-Cycle Variations of the Equivalence Ratio and Residual Gas of the Initial Charge," SAE Paper 941880, 1994.

39. Belmont, M.R., Hancock, M.S., and Buckingham, D.J., "Statistical Aspects of Cyclic Variability," SAE Paper 860324, 1986.

40. Martin, J.K., Plee, S.L., and Remboski, Jr., D.J., "Burn Modes and Prior-Cycle Effects on Cyclic Variations in Lean-Burn Spark-Ignition Engine Combustion," SAE Paper 880201, 1988.

41. Shayler, P.J., Stevens, S., and Ma, T.H., "An Analysis of Intra-Cycle and Inter-Cycle Correlations Between Combustion Parameters for a Spark Ignition Engine," IMechE Paper C465/021, 1993.

42. Stevens, S., Shayler, P.J., and Ma, T.H., "A Basis for the Predictive Control of Cyclic Dispersion in a spark Ignition Engine," IMechE Paper C448/058, 1992.

43. Pischinger, S., "Effects of Spark Plug Design on Ignition and Flame Development in an SI-Engine," Ph.D. Thesis, Mech. Eng. Dept., MIT, 1989.

44. Hoard, J., and Rehagen, L., "Relating Subjective Idle Quality to Engine Combustion," SAE Paper 970035, 1997.

45. Matthews, R.D., Sarwar. M.G., Hall, M.J., Filipe, D.J., Miller, D.L., and Cernansky, N.P., "Predictions of Cyclic Variability in an SI Engine and Comparisons with Experimental Data," SAE Paper 912345, 1991.

46. Brehob, D.D. and Newman, C.E., "Monte Carlo Simulation of Cycle by Cycle Variability," SAE Paper 922165, 1992.

47. Stone, C.R., Brown, A.G., and Beckwith, P., "Cycle-by-Cycle Variations in Spark Ignition Engine Combustion - Part II: Modelling of Flame Kernel Displacements as a Cause of Cycle-by-Cycle Variations," SAE Paper 960613, 1996.

48. Holmström, K. and Denbratt, I., "Cyclic Variation in an SI Engine Due to the Random Motion of the Flame Kernel," SAE 961152, 1996.

49. Shen, H., Hinze, P.C., and Heywood, J.B., "A Study of Cycle-to-Cycle Variations in SI Engines Using a Modified Quasi-Dimensional Model," SAE Paper 961187, 1996.

50. Ma, F., Shen, H., Liu, C., Wu, D., Li, G., and Jiang, D., "The Importance of Turbulence and Initial Flame Kernel Center Position on the Cyclic Combustion Variations for Spark-Ignition Engine," SAE Paper 961969, 1996.

51. Poulos, S.G., "The Effect of Combustion Chamber Geometry on S.I. Engine Combustion Rates - a Modeling Study," M.S. Thesis, Mech. Eng. Dept. MIT, 1982.

52. Poulos, S.G. and Heywood, J.B., "The Effect of Chamber Geometry on Spark-Ignition Engine Combustion," SAE Paper 830334, *SAE Transactions*, Vol. **92**, 1983.

53. Shen, H., Hinze, P.C., and Heywood, J.B., "A Model for Flame Initiation and Early Development in SI Engines and Its Application to Cycle-to-Cycle Variations," SAE Paper 942049, *SAE Transactions*, Vol. **103**, 1994.

54. Herweg, R. and Maly, R.R., "A Fundamental Model for Flame Kernel Formation in S.I. Engines," SAE Paper 922243, *SAE Transactions*, Vol. **101**, 1992.

55. Dai, W., Davis, G.C., Hall, M.J., and Matthews, R.D., "Diluents and Lean Mixture Combustion Modeling for SI Engines with a Quasi-Dimensional Model," SAE Paper 952382, 1995.

56. Beretta, G.P., Rashidi, M., and Keck, J.C., "Turbulent Flame Propagation and Combustion in Spark Ignition Engines," Combustion and Flame **52**, pp. 217-245, 1983.

57. Hinze, P.C., and Cheng, W.K., "Flame Kernel Development in a Methanol Fueled Engine," SAE Paper 932649, *SAE Transactions*, Vol. **102**, 1993.

58. Fox, J.W., Min, K.D., Cheng, W.K., and Heywood, J.B., "Mixture Preparation in a SI Engine with Port Fuel Injection During Starting and Warm-Up," SAE Paper 922170, *SAE Transactions*, Vol. **101**, 1992.

59. Randolph, A.L., "Methods of Processing Cylinder-Pressure Transducer Signals to Maximize Data Accuracy," SAE Paper 900170, 1990.

60. Lancaster, D.R., Krieger, R.B., and Lienesch, J.H., "Measurements and Analysis of Engine Pressure Data," SAE Paper 750026, 1975.

61. Amann, C.A., "Cylinder-Pressure Measurement and Its Use in Engine Research," SAE Paper 852067, 1985.

62. Stein, R.A., Mencik, D.Z., and Warren, C.C., "Effect of Thermal Strain on Measurement of Cylinder Pressure," SAE Paper 870455, 1987.

63. Ford Motor Company, "Acquisition and Analysis of Cylinder Pressure Data: Recommended Procedures," August 1992.

64. Cheung, H.M., "A Practical Burn Rate Analysis for Use in Engine Development and Design," M.S. Thesis, Mech. Eng. Dept. MIT, 1993.

65. *Jannaf Thermochemical Tables*, 2d ed., NSRDS-NB537, U.S. National Bureau of Standards, June 1971.